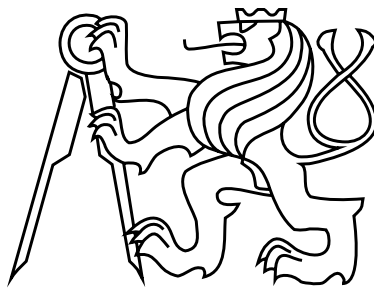


CZECH TECHNICAL UNIVERSITY IN PRAGUE

FACULTY OF CIVIL ENGINEERING

STUDY PROGRAM: GEODESY AND CARTOGRAPHY

STUDY BRANCH: GEOMATICS



MASTER'S THESIS

Application of the Finite Element Method in Physical Geodesy

Thesis supervisor: Mgr. Milan BOŘÍK, Ph.D.

Department of Mathematics

January 2017

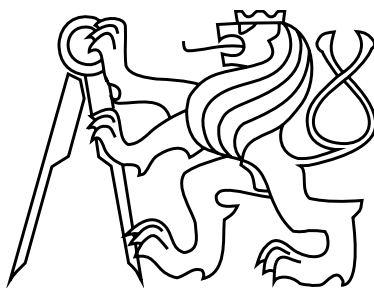
Bc. David MRÁZ

ČESKÉ VYSOKÉ UČENÍ TECHNICKÉ V PRAZE

FAKULTA STAVEBNÍ

STUDIJNÍ PROGRAM: GEODÉZIE A KARTOGRAFIE

OBOR: GEOMATIKA



DIPLOMOVÁ PRÁCE

Aplikace metody konečných prvků ve fyzikální geodésii

Vedoucí práce: Mgr. Milan BOŘÍK, Ph.D.

Katedra Matematiky

Leden 2017

Bc. David MRÁZ



ZADÁNÍ DIPLOMOVÉ PRÁCE

I. OSOBNÍ A STUDIJNÍ ÚDAJE

Příjmení: Mráz Jméno: David Osobní číslo: 381477
Zadávající katedra: 11101 Katedra matematiky
Studijní program: Geodézie a kartografie
Studijní obor: Geomatika

II. ÚDAJE K DIPLOMOVÉ PRÁCI

Název diplomové práce: Aplikace metody konečných prvků ve fyzikální geodézii
Název diplomové práce anglicky: Application of the finite element method in physical geodesy

Pokyny pro vypracování:

Nowadays global solutions of the boundary value problems in physical geodesy are mostly solved using expansion into a series of spherical harmonics. On the other hand, in regional studies, other methods, like the Fast Fourier Transform or the least square collocation, are also successfully used. We can also solve the boundary value problem in a way that allows us to look for the so-called weak solution and solve the boundary value problem with some variational methods. As computational power has increased, research is focusing more on these ways of gravity field modelling. The objective of this diploma thesis is to study application of the finite element method for solving boundary value problems in physical geodesy.

Seznam doporučené literatury:

- 1) Axelsson O, Barker V.A (2001), Finite element solution of boundary value problems: theory and computation, Society for Industrial and Applied Mathematics, Philadelphia, PA
- 2) Babuška I, Dorr MR (1981) Error estimates for the combined h and p version of finite element method. Numer Math 37:252–277
- 3) Babuška I, Suri M (1990) The p- and h-p versions of the finite element method an overview. In: Canuto C, Quarteroni A (eds) Spectral and high order methods for partial differential equations. North-Holland, Amsterdam, pp 5–26
- 4) Babuška I, Szabo B (1982) On the rates of convergence of the finite element method. Int J Numer Methods Eng 18:323–341. doi:10.1002/nme.1620180302
- 5) Ergatoudis J, Irons B, Zienkiewicz O (1968) Curved, isoparametric, quadrilateral elements for finite element analysis. Int J Solids Struct 4:31–42
- 6) Heck B (1989) On the non-linear geodetic boundary value problem for a fixed boundary surface. Bull Geod 63(1):57–67
- 7) Hofmann-Wellenhof B, Moritz H (2005) Physical geodesy. Springer, New York
- 8) Holota P, Nesvadba O (2007) Model refinements and numerical solutions of weakly formulated boundary-value problems in physical geodesy. In: Xu P, Liu J, Dermanis A (eds) VI Hotine-Marussi symposium of theoretical and computational geodesy, Wuhan, 29 May–2 June, 2006. IAG symposia, vol 132. Springer, Berlin, pp 314–320
- 9) Meissl P (1981) The use of finite elements in physical geodesy. Report 313, Geodetic Science and Surveying, The Ohio State University
- 10) Mráz D, Bořík M, Novotný J (2016) On the Convergence of the h-p Finite Element Method for Solving Boundary Value Problems in Physical Geodesy, In: International Association of Geodesy Symposia, Springer Berlin Heidelberg, doi: 10.1007/13452016237
- 11) Nesvadba O, Holota P, Klees R (2007) A direct method and its numerical interpretation in the determination of the Earth's gravity field from terrestrial data. In: Tregoning P, Rizos C (eds) Dynamic planet. International association of geodesy symposia, vol 130. Springer, Heidelberg, pp 370-376

Publishing Company, Dordrecht

13) Roy K.K (2008), Potential Theory in Applied Geophysics, Springer-Verlag Berlin Heidelberg


14) Sansò F, Sideris M (2013) Geoid determination - theory and methods. Lecture notes in earth system sciences. Springer, Heidelberg

Jméno vedoucího diplomové práce: Mgr. Milan Bořík, Ph.D.

Datum zadání diplomové práce: 3. 10. 2016

Termín odevzdání diplomové práce: 8. 1. 2017

Údaj uveďte v souladu s datem v časovém plánu příslušného ak. roku


Podpis vedoucího práce


Podpis ved

III. PŘEVZETÍ ZADÁNÍ

Beru na vědomí, že jsem povinen vypracovat diplomovou práci samostatně, bez cizí pomoci, s výjimkou poskytnutých konzultací. Seznam použité literatury, jiných pramenů a jmen konzultantů je nutné uvést v diplomové práci a při citování postupovat v souladu s metodickou příručkou ČVUT „Jak psát vysokoškolské závěrečné práce“ a metodickým pokynem ČVUT „O dodržování etických principů při přípravě vysokoškolských závěrečných prací“.

4.10.2016

Datum převzetí zadání


Podpis studenta(ky)



ZADÁNÍ DIPLOMOVÉ PRÁCE

I. OSOBNÍ A STUDIJNÍ ÚDAJE

Příjmení: Mráz Jméno: David Osobní číslo: 381477

Zadávající katedra: 11101 Katedra matematiky

Studijní program: Geodézie a kartografie

Studijní obor: Geomatika

II. ÚDAJE K DIPLOMOVÉ PRÁCI

Název diplomové práce: Aplikace metody konečných prvků ve fyzikální geodézii

Název diplomové práce anglicky: Application of the finite element method in physical geodesy

Pokyny pro vypracování:

V dnešní době je řešení okrajových úloh ve fyzikální geodézii obvykle realizováno rozvojem do řady sférických funkcí. V regionálních studiích bývá častěji aplikována např. rychlá Fourierova transformace anebo kolokační metoda s užitím nejmenších čtverců. Okrajovou úlohu lze také řešit některou z variačních metod pomocí slabé formulace. S neustálým zvyšováním výpočetního výkonu se výzkum mnohem více soustředí na využití např. metody konečných prvků. Cílem této diplomové práce je studium aplikace metody konečných prvků ve fyzikální geodézii.

Seznam doporučené literatury:

- 1) Axelsson O, Barker V.A (2001), Finite element solution of boundary value problems: theory and computation, Society for Industrial and Applied Mathematics, Philadelphia, PA
- 2) Babuška I, Dorr MR (1981) Error estimates for the combined h and p version of finite element method. Numer Math 37:252–277
- 3) Babuška I, Suri M (1990) The p- and h-p versions of the finite element method an overview. In: Canuto C, Quarteroni A (eds) Spectral and high order methods for partial differential equations. North-Holland, Amsterdam, pp 5–26
- 4) Babuška I, Szabo B (1982) On the rates of convergence of the finite element method. Int J Numer Methods Eng 18:323–341. doi:10.1002/nme.1620180302
- 5) Ergatoudis J, Irons B, Zienkiewicz O (1968) Curved, isoparametric, quadrilateral elements for finite element analysis. Int J Solids Struct 4:31–42
- 6) Heck B (1989) On the non-linear geodetic boundary value problem for a fixed boundary surface. Bull Geod 63(1):57–67
- 7) Hofmann-Wellenhof B, Moritz H (2005) Physical geodesy. Springer, New York
- 8) Holota P, Nesvadba O (2007) Model refinements and numerical solutions of weakly formulated boundary-value problems in physical geodesy. In: Xu P, Liu J, Dermanis A (eds) VI Hotine-Marussi symposium of theoretical and computational geodesy, Wuhan, 29 May–2 June, 2006. IAG symposia, vol 132. Springer, Berlin, pp 314–320
- 9) Meissl P (1981) The use of finite elements in physical geodesy. Report 313, Geodetic Science and Surveying, The Ohio State University
- 10) Mráz D, Bořík M, Novotný J (2016) On the Convergence of the h-p Finite Element Method for Solving Boundary Value Problems in Physical Geodesy, In: International Association of Geodesy Symposia, Springer Berlin Heidelberg, doi: 10.1007/13452016237
- 11) Nesvadba O, Holota P, Klees R (2007) A direct method and its numerical interpretation in the determination of the Earth's gravity field from terrestrial data. In: Tregoning P, Rizos C (eds) Dynamic planet. International association of geodesy symposia, vol 130. Springer, Heidelberg, pp 370-376
- 12) Rektorys K (1980) Variational methods in mathematics, science and engineering. D. Reidel

13) Roy K.K (2008), Potential Theory in Applied Geophysics, Springer-Verlag Berlin Heidelberg

14) Sansò F, Sideris M (2013) Geoid determination - theory and methods. Lecture notes in earth system sciences. Springer, Heidelberg

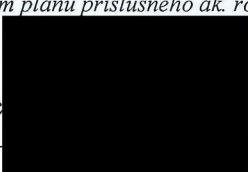
Jméno vedoucího diplomové práce: Mgr. Milan Bořík, Ph.D.

Datum zadání diplomové práce: 3. 10. 2016

Termín odevzdání diplomové práce: 8. 1. 2017

Údaj uveďte v souladu s datem v časovém plánu příslušného ak. roku


Podpis vedoucího práce


Podpis vedoucího práce

III. PŘEVZETÍ ZADÁNÍ

Beru na vědomí, že jsem povinen vypracovat diplomovou práci samostatně, bez cizí pomoci, s výjimkou poskytnutých konzultací. Seznam použité literatury, jiných pramenů a jmen konzultantů je nutné uvést v diplomové práci a při citování postupovat v souladu s metodickou příručkou ČVUT „Jak psát vysokoškolské závěrečné práce“ a metodickým pokynem ČVUT „O dodržování etických principů při přípravě vysokoškolských závěrečných prací“.

4.10.2016

Datum převzetí zadání


Podpis studenta(ky)

Abstract

A geopotential model of the Earth is usually calculated using the Stokes coefficients. As computational power has increased, research is focusing more on new ways of precise gravity field modelling. The objective of this master's thesis is to study an application of the h-p finite element method for solving boundary value problems in physical geodesy. The brief introductions to potential theory, gravity field of the Earth and h-p finite element method are in chapters 2-4. Chapters 5-8 are dedicated to my research. For the purpose of studying the method, the model boundary value problems with the corresponding finite element discretization were formulated. The algorithm for solving these boundary value problems was designed and subsequently implemented by the program. The isoparametric reference elements with linear and quadratic shape functions is used. We apply the h and p methodologies for increasing the rate of convergence of the weak solution, discuss mesh generation for large domains and also solve linear system with various direct methods. The methodologies for increasing the rate of convergence are applied on the computation of the global solution of the geodetic boundary value problem, where the input data on the surface of the Earth are prescribed using the Earth Gravitational Model (EGM2008).

Keywords: boundary value problem, geodetic boundary value problem, gravity field modelling, isoparametric reference element, h-p finite element method, Poisson's equation, physical geodesy

Abstrakt

V dnešní době je geopotenciální model Země obvykle počítán pomocí Stokesových koeficientů. S neustálým zvyšováním výpočetního výkonu se výzkum stále více soustředí na nové způsoby přesného určování tíhového pole Země. Cílem této diplomové práce je studium aplikace h-p metody konečných prvků na řešení okrajových úloh ve fyzikální geodézii. Kapitoly 2-4 slouží jako úvod do problematiky určování gravitačního pole Země a metody konečných prvků. Kapitoly 5-8 jsou pak určeny mého výzkumu. Za účelem studia konvergence metody jsem nejprve formuloval modelové okrajové úlohy pro rozdílné okrajové podmínky a také odpovídající diskretizaci pomocí metody konečných prvků. Algoritmus pro řešení těchto úloh byl navržen a následně implementován programem. Na řešení úloh je použit isoparametrický referenční prvek s lineárními a kvadratickými funkcemi. V rámci práce řeším řadu okrajových úloh, aplikuji h a p metodologii na zvýšení rychlosti konvergence slabého řešení, probírám generování sítí konečných prvků pro velké domény a také řeším systémy lineárních rovnic pomocí různorodých přímých metod. Metody na zvýšení rychlosti konvergence jsou pak aplikovány na výpočet globálního řešení geodetické okrajové úlohy, kde jsou data na povrchu Země předepsána pomocí Zemského Gravitačního Modelu (EGM2008).

Klíčová slova: okrajová úloha, geodetická okrajová úloha, modelování tíhového pole, isoparametrický referenční prvek, h-p metoda konečných prvků, Poissonova rovnice, fyzikální geodézie

Acknowledgments

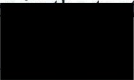
I would like to express thanks to Mgr. Milan Bořík, Ph.D. for his assistance, support and advices on this topic. I would like to also thanks to Ing. Jan Holešovský for his consultation on the gravity data available for the Czech Republic. Some cited resources and research were supported by the Grant Agency of the Czech Technical University in Prague by grant No. SGS OHK1-016/15.

Poděkování

Chtěl bych poděkovat Mgr. Milanu Boříkovi, Ph.D. za podporu a cenné rady na toto téma. Chtěl bych také poděkovat Ing. Janu Holešovskému za konzultaci ohledně dostupných tíhových dat pro Českou republiku. Některé citované zdroje a výzkumy byly podpořeny Grantovou Agenturou Českého Vysokého Učení Technického v Praze grantem č. SGS OHK1-016/15.


Statement of Academic Honesty

I herewith declare that the submitted master's thesis with the title "Application of the finite element method in physical geodesy" has been created by myself without any inadmissible help and without the use of sources other than those given due reference and listed in the list of references

Place and date Prague 8.1.2017 Signature 

Prohlášení

Prohlašuji, že jsem diplomovou práci na téma "Application of the finite element method in physical geodesy" vypracoval samostatně. Použitou literaturu a podkladové materiály uvádím v seznamu zdrojů.

Místo a datum Praha 8.1.2017 Podpis autora 

Contents

1	Introduction	17
2	Potential theory	19
2.1	Fundamentals	19
2.2	Poisson equation	20
3	Gravity field of the Earth	23
3.1	Gravity potential	23
3.2	Normal and disturbing potential	25
3.3	Geodetic boundary value problem	27
4	h-p Finite element method	29
4.1	Weak formulation	29
4.2	h-p FEM discretization	32
5	Software design	35
5.1	Overview	35
5.2	Mesh generation	36
5.3	Numerical integration	37
5.4	Reference element	39
5.5	Mapping the reference element to global coordinates	41
5.6	Assembling	44
5.7	Solving linear system	47

6	Numerical experiments	49
6.1	Overview	49
6.2	Formulations of boundary value problems from the first category	50
6.2.1	First problem	50
6.2.2	Second problem	51
6.2.3	Third problem	52
6.3	Formulations of the boundary value problems of the second category (global solution)	53
7	Results	55
7.1	Solution of the linear system	55
7.2	Convergence experiments	57
7.3	Global solution	62
8	Conclusion	65

List of Figures

4-1	Reference elements in local coordinates ψ, φ, ϑ a) Isoparametric reference element with linear shape functions (IRELSF) b) Isoparametric reference element with quadratic shape functions (IREQSF)	32
5-1	Simplified scheme of the potential calculation	36
5-2	Distribution of the Gauss points on each element for the computation of triple integrals in stiffness matrices (5.6)	38
5-3	Mesh for model example	43
6-1	Finite element mesh for the first category BVPs with quadratic shape functions and depicted boundary conditions	50
6-2	Methodology for choosing boundary condition on the simple finite element mesh .	54
7-1	The structure of the stiffness matrix for convergence experiments (This example is made for the mesh, where the domain is discretized by thirty elements in radial direction)	56
7-2	The structure of the stiffness matrix for basic example of the global solution, see Fig. 7-8	57
7-3	Increasing convergence with the h methodology. The linear shape functions are used. The meshes are generated with the constant radial size of each element. The domain is bounded with the top boundary $\rho_{TOP} = \rho_{DEMO}$	58
7-4	Increasing the convergence rate using the p methodology with 5 elements in radial direction with linear and also quadratic shape functions	59

7-5	The relative error for different mesh generation. The domain is bounded by $\rho_{TOP} = \rho_{DEMO} = 10^9$. In these cases we solve the Laplace equation with the isoparametric reference element with linear shape functions	60
7-6	a) Finding the threshold point with minimum relative error on the mesh with 30 elements b) Finding the distribution of the elements in radial direction with the minimum relative error on the mesh with 30 elements	61
7-7	The overall absolute differences for the solution of the model BVP in Sec. 6.2.2 with the Dirichlet condition W_{SURF} on the bottom boundary. The domain is in radial direction bounded by ρ_{SURF} and ρ_{SAT} . The mesh was generated with the constant radial size of the element. The isoparametric reference element with linear shape functions is used.	61
7-8	Global solution for the gravitational potential V , where the Dirichlet boundary conditions are prescribed on the surface and the top boundary. The domain is discretized by 5 element in terms of radial direction and bounded by $\rho_{TOP} = 10^9$. Reference surface is the sphere with the mean radius of the Earth.	62
7-9	Detail on the generating mesh on the poles a) overview b) profile c) perspective. For illustrative purpose the angle, which defines spherical trapesoid in terms of λ and φ , is equal to 20 degrees. However in the computation of the geodetic boundary value problem is the angle equal to 0.0002.	63
7-10	Computation of the gravity potential W . The problem is formulated as the geodetic boundary value problem in Sec. 6.3. On the Surface's of the Earth the Neumann condition with the magnitudes of the gravity acceleration g is prescribed. The oblique derivative effect was neglected.	64

List of Tables

2.1	Physical constants	19
3.1	Parameters of the WGS 84 reference ellipsoid	27
5.1	Weight of Gauss points	38
6.1	Parameters for the domain Ω	51
7.1	The time elapsed for solving the linear system using the various methods. The domain is discretized by 1000 elements in radial direction.	56
7.2	Relative errors for different mesh generation with the dependence on the number of elements in radial direction	60
7.3	Example of the output from the official FORTRAN program	63

Chapter 1

Introduction

Nowadays the global solutions of the boundary value problems (BVPs) in physical geodesy are mostly solved using the expansion into the series of spherical harmonics (Hoffmann-Wellenhof et al. 2005). On the other hand, in regional studies other methods like the Fast Fourier Transform or the least square collocation are also successfully used (Sansò et al. 2013).

We can also solve the BVP in a way, that we are looking for the so-called weak solution (Rektorys 1980) and solve the BVP with some variational method. The first work published on the application of the finite element method (FEM) in geodesy was done by Meissl (1981), followed by Shaofeng and Dingbo (1991). Recently, Galerkin method, FEM and hp-FEM are discussed in Holota (2000,2001,2005), Holota et al. (2007), Nesvadba et al. (2007), Fašková et al. (2010), Šprlák et al. (2011), Mráz et al. (2015a, 2015b) and Mráz et al. (2016). Besides that, the boundary element method (Klees 1995; Klees et al. 2001; Čunderlík et al. 2008) and the finite volume method in Minarechová et al. (2015) were also efficiently used. The aim of this master's thesis is to study the application of the h-p FEM (Babuška et al. 1990) for the different boundary value problems on different domains and prepare the methodology for computing high resolution gravity field model.

Chapter 2

Potential theory

2.1 Fundamentals

Let us have two point masses S and P , where the mass is denoted as M and m . The point mass S is the source body of gravitation and the point mass P is the attracted point. Let xyz is rectangular system, where S has coordinates ξ, η, ϑ and P has coordinates x, y, z . The distance between the point masses S and P is r and \mathbf{r}_{SP} is the position vector

$$r = \sqrt{(x - \xi)^2 + (y - \eta)^2 + (z - \vartheta)^2}. \quad (2.1)$$

According to Newton's law of gravitation (Hoffmann-Wellenhof et al. 2005) two points S and P attract each other with a force

$$F = G \frac{Mm}{r^2}, \quad (2.2)$$

where G is Newton's gravitational constant, see Tab. 2.1. The masses M and m attract each other in the symmetrical way, but it is convenient to say, that the force \mathbf{F} with the magnitude F is exerted

Name	Label	Value	Units
Newton's Gravitational constant	G	$6.6742 \cdot 10^{-11}$	$m^3 kg^{-1} s^{-2}$
Standar gravitational parameter for Earth	GM	$3.986004418(9) \cdot 10^{14}$	$m^3 s^{-2}$
Angular velocity	ω	7.2921159×10^{-5}	$\frac{rad}{s}$

Table 2.1: Physical constants

by the mass M .

$$\mathbf{F}_{SP} = -G \frac{Mm}{r^3} \mathbf{r}_{SP}. \quad (2.3)$$

For simplicity consider, that the attracted mass point P has the mass m equal to unity. This function is called intensity of the gravitational field

$$\mathbf{K} = \frac{\mathbf{F}}{m} = -G \frac{M}{r^3} \mathbf{r}_{SP}. \quad (2.4)$$

Now introduce a new scalar function, which is defined as follows

$$V = \frac{GM}{r} \quad [m^2 s^{-2}]. \quad (2.5)$$

This scalar function is called gravitational potential or potential of gravitation and the relation between the intensity of the gravitational field and the gravitational potential is

$$\mathbf{K} = \nabla V, \quad (2.6)$$

which can be easily proofed by differentiating, see Zeman (2005) or Roy (2008). A very important property of the potential is that for a system of n point masses M_1, M_2, \dots, M_n , the potential is the sum of the individual contributions. The final potential equals to

$$V = \frac{GM_1}{r_1} + \frac{GM_2}{r_2} + \dots + \frac{GM_n}{r_n} = \sum_i^n G \frac{M_i}{r_i}. \quad (2.7)$$

In physics and geodesy we have to take into account the fact, that potential is regular at infinity and converges to zero

$$\lim_{r \rightarrow \infty} V(x, y, z) = 0. \quad (2.8)$$

2.2 Poisson equation

If we assume that the point masses are distributed continuously over a volume v of the source body S with the surface Σ . For a mass of solid body M , which substitutes source point mass S , we can

write

$$M = \iiint_{\mathfrak{v}} \sigma(x, y, z) \, dx dy dz, \quad (2.9)$$

where $\sigma(x, y, z)$ is the density of the solid body S . If we consider (2.7) and substitute (2.9) for M the gravitational potential V can be expressed as

$$V(x, y, z) = G \iiint_{\mathfrak{v}} \frac{\sigma(x, y, z)}{\sqrt{(x - \xi)^2 + (y - \eta)^2 + (z - \vartheta)^2}} dx dy dz. \quad (2.10)$$

It is well known that integration over the solid angle of the unit sphere is equal to

$$\iint_{\Sigma} \frac{\mathbf{r} \cdot \mathbf{n}}{r^3} d\Sigma = 4\pi. \quad (2.11)$$

Now for the surface Σ of the solid body S define the flux of \mathbf{K} over the surface Σ

$$\iint_{\Sigma} \mathbf{K} \cdot d\mathbf{\Sigma} = \iint_{\Sigma} \mathbf{K} \cdot \mathbf{n} d\Sigma, \quad (2.12)$$

where \mathbf{K} is a gravitational vector field (2.4). With substituting (2.3), (2.11) to (2.12) we get

$$\iint_{\Sigma} \mathbf{K} \cdot \mathbf{n} d\Sigma = -GM \iint_{\Sigma} \frac{\mathbf{r} \cdot \mathbf{n}}{r^3} d\Sigma = -4\pi GM. \quad (2.13)$$

Using the divergence theorem (Rektorys 1994) we can also write

$$\iint_{\Sigma} \mathbf{K} \cdot d\mathbf{\Sigma} = \iiint_{\mathfrak{v}} \nabla \mathbf{K} \, dx dy dz = -4\pi G \iiint_{\mathfrak{v}} \sigma(x, y, z) \, dx dy dz. \quad (2.14)$$

Considering (2.6) we can write the relation

$$\iiint_{\mathfrak{v}} \nabla \cdot \nabla V \, dx dy dz = -4\pi G \iiint_{\mathfrak{v}} \sigma(x, y, z) \, dx dy dz, \quad (2.15)$$

which is equal to the so-called Poisson's equation

$$\Delta V = \frac{\partial^2 V}{\partial x^2} + \frac{\partial^2 V}{\partial y^2} + \frac{\partial^2 V}{\partial z^2} = -4\pi G \sigma(x, y, z), \quad (2.16)$$

where Δ is the Laplace's operator

$$\Delta = \nabla \cdot \nabla = \frac{\partial^2}{\partial x^2} + \frac{\partial^2}{\partial y^2} + \frac{\partial^2}{\partial z^2}. \quad (2.17)$$

The Poisson's equation is partial differential equation of elliptic type (Evans L C 1998). In potential theory the fundamental problem is the Dirichlet problem. The problem is to find a potential in domain Ω , given its continuous restriction

$$V(x, y, z) = f(x, y, z), \quad (2.18)$$

to the boundary $\partial\Omega = \Gamma$ of the domain Ω . And also with the assumption that the mass distribution in the interior of the domain Ω is known. The Dirichlet boundary value problem is used in one of the experiments in Sec. 6.2.2. The second boundary value problem or the Neumann problem is to find potential in Ω with the restriction of normal derivative

$$\frac{\partial V(x, y, z)}{\partial n} = f(x, y, z). \quad (2.19)$$

However in geodesy arise boundary value problems with the so-called oblique derivative effect. In the oblique derivative problem the normal derivative is replaced by derivative $\frac{\partial V(x, y, z)}{\partial l}$ with respect to an arbitrary direction $l = l(x, y, z)$. However if the direction of the derivative is normal to the boundary surface, the oblique derivative effect is transformed to the Neumann problem. The last boundary value problem is the problem with Robin boundary conditions, where the linear combination of the values of a function and the values of its derivative on the boundary of the domain is used

$$\alpha \frac{\partial V(x, y, z)}{\partial n} + \beta V(x, y, z) = f(x, y, z), \quad (2.20)$$

where $\alpha, \beta \in \mathbb{R}$ are constants. The Robin boundary conditions are used in the numerical experiments of the first and second category, see Sec. 6.2.1, Sec.6.2.2.

Chapter 3

Gravity field of the Earth

3.1 Gravity potential

Now assume, that we will compute gravitational potential only for an exterior of the source body S and also consider, that the source body S is the Earth and the density of the atmosphere is neglected.

We can modify the Poisson's equation (2.16) to the form of Laplace's equation

$$\Delta V = \left(\frac{\partial^2 V}{\partial x^2} + \frac{\partial^2 V}{\partial y^2} + \frac{\partial^2 V}{\partial z^2} \right) = 0. \quad (3.1)$$

The solutions of the Laplace's equation are harmonic functions. The general definition is that the harmonic function is a twice differentiable function $f : U \rightarrow \mathbb{R}$, where U is an open subset of \mathbb{R}^n . Nevertheless the solution is harmonic only outside of the attracting masses, where the Laplace's equation is valid, but not inside, where the Poisson's equation is valid. It can be also shown, that every harmonic function is analytic in the region Ω , where satisfies the Laplace's equation and that is continuous and has continuous derivatives of any order. In order to describe positions in space and field quantities for the Earth we introduce an Earth-fixed, orthonormal coordinate frame. It is postulated that the origin 0 is situated near the Earth's center of mass. Its z -axis coincides with the Earth's mean axis of rotation and the Greenwich meridian plane is parallel to x -axes. The y -axis completes the orthonormal global geocentric rectangular system, which is oriented in mathematically positive sense. The distance from the attracting mass S and potential point P has been already defined (2.1). The longitude λ and the latitude φ of the potential point P than satisfy

the conditions $0 \leq \lambda \leq 2\pi$ and $-\pi \leq \varphi \leq \pi$. Now define intensity of the centrifugal force K_Φ . The magnitude than is

$$K_\Phi = \omega^2 \sqrt{x^2 + y^2}, \quad (3.2)$$

where ω is the angular velocity of the Earth, see Tab. 2.1. The centrifugal intensity is generated by the Earth's rotation and the relationship

$$\mathbf{K}_\Phi = \nabla\Phi \quad (3.3)$$

is also valid for the centrifugal intensity. In the relation (3.3) we denote Φ as centrifugal potential, which is given by

$$\Phi = \frac{1}{2} \omega^2 (x^2 + y^2). \quad (3.4)$$

By the differentiating of the centrifugal potential we can find, that centrifugal potential is not harmonic. Laplacian of the centrifugal potential is $2\omega^2$, hence Φ satisfies the Poisson's equation

$$\Delta\Phi = \left(\frac{\partial^2\Phi}{\partial x^2} + \frac{\partial^2\Phi}{\partial y^2} + \frac{\partial^2\Phi}{\partial z^2} \right) = 2\omega^2. \quad (3.5)$$

The potential of gravity is called gravity potential W and the resultant is obtained by adding gravitational potential V and centrifugal potential Φ

$$W = V + \Phi. \quad (3.6)$$

Also for gravity vector is true, that gradient of the gravity potential is equal to gravity vector

$$\mathbf{g} = \nabla W. \quad (3.7)$$

Gravity vector \mathbf{g} is always normal to equipotential surface $W = \text{const}$. The orthogonal trajectories are denoted as plumb lines. Gravity vector \mathbf{g} is tangent to the plumb line at the potential point P . If we consider, that centrifugal potential satisfies the Poisson's equation, than for general gravity

potential W we get

$$\Delta W = \left(\frac{\partial^2 W}{\partial x^2} + \frac{\partial^2 W}{\partial y^2} + \frac{\partial^2 W}{\partial z^2} \right) = -4\pi G\sigma(x, y, z) + 2\omega^2. \quad (3.8)$$

Again we deal only with the exterior of the Earth so the Poisson's equation can be modified as

$$\Delta W = \left(\frac{\partial^2 W}{\partial x^2} + \frac{\partial^2 W}{\partial y^2} + \frac{\partial^2 W}{\partial z^2} \right) = 2\omega^2. \quad (3.9)$$

3.2 Normal and disturbing potential

This section is intended to be more as a brief review of the basic relationships, which have to be defined in order to obtain the data for the geodetic boundary value problem. For more detailed information is more sufficient to read e.g. Hoffmann-Wellenhof et al. (2005). In geodesy the normal potential for the spherically symmetrical body is defined as follows

$$U = \frac{GM}{r}. \quad (3.10)$$

It is also true, that the gradient of the normal potential is equal to normal gravity vector

$$\gamma = \nabla U. \quad (3.11)$$

We can subtract gravity potential from the normal potential and obtain so-called disturbing or anomalous potential T

$$T = W - U. \quad (3.12)$$

Disturbing potential is harmonic, therefore satisfies the Laplace's equation

$$\Delta T = \left(\frac{\partial^2 T}{\partial x^2} + \frac{\partial^2 T}{\partial y^2} + \frac{\partial^2 T}{\partial z^2} \right) = 0. \quad (3.13)$$

The geoid undulation N is expressed in a form of Brun's theorem or Stoke's integral. This allow us to define relation between measurable free-air anomaly Δg

$$\Delta g = \nabla T = g - \gamma \quad (3.14)$$

and unkown disturbing potential T . However the relation 3.10 is only the first approximation, the second approximation is the reference ellipsoid. In this master's thesis WGS84 ellipsoid is used. The cartesian coordinates can be calculated using the relations

$$\begin{aligned} x &= \left(\frac{a^2}{\sqrt{a^2 \cos^2 \varphi + b^2 \sin^2 \varphi}} + h \right) \cos \varphi \cos \lambda, \\ y &= \left(\frac{a^2}{\sqrt{a^2 \cos^2 \varphi + b^2 \sin^2 \varphi}} + h \right) \cos \varphi \sin \lambda, \\ z &= \left(\frac{b^2}{a^2} \frac{a^2}{\sqrt{a^2 \cos^2 \varphi + b^2 \sin^2 \varphi}} + h \right) \sin \varphi, \end{aligned} \quad (3.15)$$

where h is ellipsoidal height, a is semi-major axis and b is semi-minor axis. Normal gravity acceleration is then defined from the Somigliana-Pizzetti formula for reference ellipsoid

$$\gamma = \gamma_e \frac{1 + k \sin^2 \varphi}{\sqrt{1 - e^2 \sin^2 \varphi}}, \quad (3.16)$$

where k is equal to

$$k = \frac{b}{a} - 1. \quad (3.17)$$

With substituting parameters for the WGS84 ellipsoid we get

$$\gamma = 9.7803253359 \frac{1 + 0.00193185265241 \sin^2 \varphi}{\sqrt{1 - 0.00669437999013 \sin^2 \varphi}} [ms^{-2}]. \quad (3.18)$$

The values of parameters for WGS84 reference ellipsoid are shown in Tab. 3.2.

Label	Name	Value	Units
a	semi-major axis	6378137.00	$[m]$
b	semi-minor axis	6356752.3142	$[m]$
e	first ellipsoidal eccentricity	$8,1819190842622 \times 10^{-2}$	$[\]$
f	flattening of WGS 84 ellipsoid	$1/298.257223563$	$[\]$
GM	Earth's standard gravitational parameter	$3.986004418 \times 10^{14}$	$[m^3 s^{-2}]$
ω	Earth's angular velocity	7292115×10^{-11}	$[\frac{rad}{s}]$
γ_e	normal gravity on equator	9.7803253359	$[\frac{rad}{s}]$
γ_p	normal gravity on the pole	9.8321849378	$[ms^{-2}]$

Table 3.1: Parameters of the WGS 84 reference ellipsoid

3.3 Geodetic boundary value problem

The equation (3.9) is the main concern of this master's thesis. We will focus primary on the GBVPs, where the unknown is gravity potential W on and outside of the boundary surface $\partial\Omega$. In this problem we assume, that the Earth behave like a rigid, non-deformable body, uniformly rotating about a space and body-fixed axis in \mathbb{R}^3 . The solution exists and is unique as it was proofed in Koch (1972). All attracting mass elements are located in the interior of the closed boundary Σ which represents the Earth's surface. We will assume, that the boundary surface is smooth in terms of Lipshitzian boundary. As we discussed in Sec. 2.1 the generated attraction of mass elements on a point mass P generates the gravitational potential V , which is regular at infinity and fulfills (3.1).

As it was mentioned for the exterior of the Earth, we have to deal with the GBVP, which satisfies the equation (3.9). On the surface of the Earth Σ the magnitudes of gravity acceleration $g = |\nabla W|$ is prescribed as the Neumann condition (2.19). On the upper boundary, see Fig. 5-3 is Dirichlet condition (2.18) prescribed as zero (for really large domain in terms of the radial direction) and prescribed as gravity potential W observed from satellites for the domain, where the upper boundary is in the height of the satellite, see Sec. 6. The boundary conditions are then mixed (2.20). In the numerical experiments, where the shape of the domain is spherical trapezoid, the additional Neumann conditions on the artificial planes are equal to zero. This can be used only for spherically symmetrical body with the constant gravity acceleration or potential on the surface. However it's valid for studying convergence tendencies of the finite element method in the radial direction.

The geodetic boundary value problems, which are based on the relationship between any boundary data and the gravity potential W are denoted fixed GBVP. In geodesy we distinguish between several types of the GBVPs. The free nonlinear and gravimetric GBVPs were discussed in Graffarend (1971), Bjerhammar et al. (1983), Grafarend et al. (1985), Grafarend (1989) and Heck (1989). The other BVPs were also discussed e.g. Hormander (1975). In this master's thesis the fixed GBVP is solved.

The problematics of the GBVPs are much more complex, for the purpose of studying h-p finite element method the problem of the observables was simplified and the data are obtained from the EGM2008. The problematics of the GBVP is explained more in detail in Sansò et al. (1997) or Sansò (2013).

Chapter 4

h-p Finite element method

4.1 Weak formulation

The formulation of the BVP was partially discussed in the description of the fixed GBVP in Sec. 3.3. In this section the BVP is formulated more precisely and also weak formulation is derived. Denote Ω an open domain in \mathbb{R}^3 . In the model problems the domain Ω is supposed to be bounded with Lipschitzian boundary $\partial\Omega = \Gamma_N \cup \Gamma_D$, where Γ_N is the Neumann boundary and Γ_D is the Dirichlet boundary. Now construct the corresponding Sobolev space (Adams 2003). Let $k \in \mathbb{N}$. $p \in [1, \infty]$ and

$$\alpha = (\alpha_1, \dots, \alpha_n), \quad |\alpha| = \sum_{i=1}^n \alpha_i, \quad D^\alpha = \frac{\partial^{|\alpha|}}{\partial x_1^{\alpha_1} \dots \partial x_n^{\alpha_n}}, \quad u^\alpha = D^\alpha u. \quad (4.1)$$

The Sobolev space is defined to be the set of all functions f defined on Ω such that for every multi-index α with $|\alpha| \leq k$, where $|\alpha| \leq k$. The mixed partial derivative exists in the weak sense and is in $L^p(\Omega)$

$$f^\alpha = \frac{\partial^\alpha f}{\partial x_1^{\alpha_1} \dots \partial x_n^{\alpha_n}}. \quad (4.2)$$

The Sobolev space $W^{k,p}$ is then constructed as

$$W^{k,p}(\Omega) = \{u \in L^p(\Omega) : D^\alpha u \in L^p(\Omega) \forall |\alpha| \leq k\} \quad (4.3)$$

and with the Sobolev norm

$$\|u\|_{W^{k,p}(\Omega)} := \begin{cases} \left(\sum_{|\alpha| \leq k} \|D^\alpha u\|_{L^p(\Omega)}^p \right)^{\frac{1}{p}} & 1 \leq p < +\infty \\ \max_{|\alpha| \leq k} \|D^\alpha u\|_{L^\infty(\Omega)} & p = +\infty \end{cases}. \quad (4.4)$$

For the purpose of the generality of the weak formulation, we consider the Poisson equation for the potential $V(x, y, z)$ in the general form

$$\left(\frac{\partial^2 V}{\partial x^2} + \frac{\partial^2 V}{\partial y^2} + \frac{\partial^2 V}{\partial z^2} \right) = -f(x, y, z), \quad (4.5)$$

where $f \in L_2(\Omega)$. In our case we derive the problem with Robin boundary conditions (2.20)

$$\begin{aligned} V(x, y, z) &= k(x, y, z) \text{ on } \Gamma_D, \\ \frac{\partial V(x, y, z)}{\partial \mathbf{n}} &= l(x, y, z) \text{ on } \Gamma_N, \end{aligned} \quad (4.6)$$

where $k(x, y, z)$ is a function representing values on the Dirichlet boundary Γ_D and $l(x, y, z)$ is a function representing values on the Neumann boundary Γ_N and \mathbf{n} is a direction of the outward unit normal with respect to $\partial\Omega$. The existence and the uniqueness of the solution can be proofed using the Lax-Milgram lemma e.g. Nečas (2003), Axelson (2001), Rektorys (1980) or Evans (1998). Now consider a test function v from the Sobolev space $W^{1,2}(\Omega)$, which is constructed using the definition (4.3) with the norm (4.4) for $p = 2$ and for the order of the Sobolev space $k = 1$. The Sobolev space $W^{1,2}$ can be also denoted as the Hilbert space $H^1(\Omega)$ with the norm $\|\cdot\|_{W^{1,2}(\Omega)}$. In geodesy we can also formulate the problem for an unbounded domain Ω . In this case the weighted Sobolev space needs to be constructed as in Sansò et al. (1997) and Holota (2007). However for a bounded the domain we can construct space $W^{1,2}$. The potential V is assumed to be regular as $\rho \rightarrow \infty$. The test function v is chosen in a way, that is equal to zero on the Dirichlet boundary

$$\vartheta_M = \{v \in W^{1,2}(\Omega), v = 0 \text{ on } \Gamma_D\}. \quad (4.7)$$

We multiply (4.5) by the test function v and integrate both sides of the equation we get

$$\int_{\Omega} \left(\frac{\partial^2 V}{\partial x^2} v + \frac{\partial^2 V}{\partial y^2} v + \frac{\partial^2 V}{\partial z^2} v \right) dx dy dz = - \int_{\Omega} f v dx dy dz, \quad (4.8)$$

using Gauss-Green theorem (Rektorys 1994)

$$\int_{\Omega} \frac{\partial f}{\partial x_{n_k}} dx = \int_{\partial\Omega} f n_k dS, \quad k = 1, \dots, n, \quad (4.9)$$

and denoting $f = \frac{\partial V}{\partial x_k}$, $g = v$ we get the relationships

$$\begin{aligned} \int_{\Omega} \frac{\partial^2 V}{\partial x^2} d\Omega &= \int_{\partial\Omega} \frac{\partial V}{\partial x} v n_x dS - \int_{\Omega} \frac{\partial V}{\partial x} \frac{\partial v}{\partial x}, \\ \int_{\Omega} \frac{\partial^2 V}{\partial y^2} d\Omega &= \int_{\partial\Omega} \frac{\partial V}{\partial y} v n_y dS - \int_{\Omega} \frac{\partial V}{\partial y} \frac{\partial v}{\partial y}, \\ \int_{\Omega} \frac{\partial^2 V}{\partial z^2} d\Omega &= \int_{\partial\Omega} \frac{\partial V}{\partial z} v n_z dS - \int_{\Omega} \frac{\partial V}{\partial z} \frac{\partial v}{\partial z}. \end{aligned} \quad (4.10)$$

And by substituting (4.10) to (4.8) we get

$$\begin{aligned} - \int_{\partial\Omega} \left(\frac{\partial V}{\partial x} n_x + \frac{\partial V}{\partial y} n_y + \frac{\partial V}{\partial z} n_z \right) v dS + \int_{\Omega} \left(\frac{\partial V}{\partial x} \frac{\partial v}{\partial x} + \frac{\partial V}{\partial y} \frac{\partial v}{\partial y} + \frac{\partial V}{\partial z} \frac{\partial v}{\partial z} \right) dx dy dz = \\ = \int_{\Omega} f v dx dy dz. \end{aligned} \quad (4.11)$$

By splitting the boundary $\partial\Omega$ we can rearrange the equation (4.11) into

$$\begin{aligned} \int_{\partial\Omega} \left(\frac{\partial V}{\partial x} n_x + \frac{\partial V}{\partial y} n_y + \frac{\partial V}{\partial z} n_z \right) v dS = \int_{\Gamma_D} \left(\frac{\partial V}{\partial x} n_x + \frac{\partial V}{\partial y} n_y + \frac{\partial V}{\partial z} n_z \right) v dS + \\ + \int_{\Gamma_N} \left(\frac{\partial V}{\partial x} n_x + \frac{\partial V}{\partial y} n_y + \frac{\partial V}{\partial z} n_z \right) v dS. \end{aligned} \quad (4.12)$$

With respect to the boundary conditions (4.7), we get the weak formulation in this form: find $V \in W^{1,2}(\Omega)$ that

$$\begin{aligned} \int_{\Omega} \left(\frac{\partial V}{\partial x} \frac{\partial v}{\partial x} + \frac{\partial V}{\partial y} \frac{\partial v}{\partial y} + \frac{\partial V}{\partial z} \frac{\partial v}{\partial z} \right) dx dy dz = \\ = \int_{\Omega} f(x, y, z) v d\Omega + \int_{\Gamma_N} l(x, y, z) v dS, \end{aligned} \quad (4.13)$$

for each $v \in \mathcal{V}_M$.

4.2 h-p FEM discretization

Finite element method in this master's thesis denotes the implementation of Galerkin method with finite element basis function. These basis function are continuous, piecewise polynomials and that have local in the sense that each function vanishes outside of a small subregion of domain Ω . Together with the choice of nodes, makes up a finite element mesh, see Fig. 5-3. The isoparametric reference elements with linear and quadratic shape function (Ergatoudis J 1968) are chosen, see Fig. 4-1.

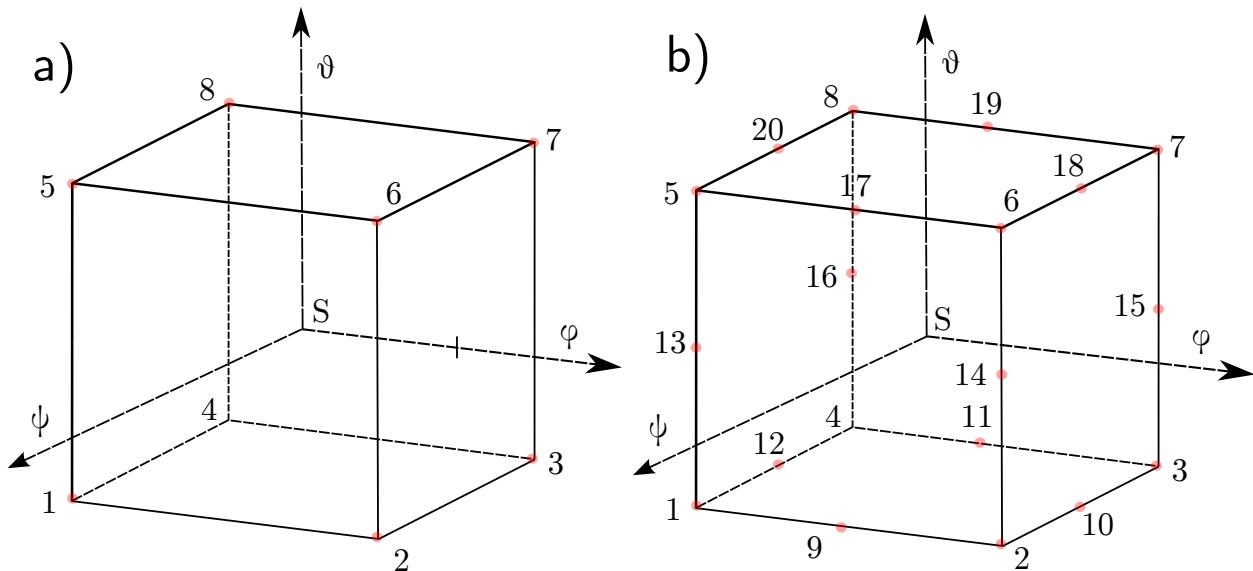


Figure 4-1: Reference elements in local coordinates ψ, ϕ, θ a) Isoparametric reference element with linear shape functions (IRELSF) b) Isoparametric reference element with quadratic shape functions (IREQSF)

In the h-p FEM we find the solution $V(x, y, z)$ as a linear combination

$$V(x, y, z) = \sum_{i=1}^n \alpha_i \varphi_i(x, y, z), \quad (4.14)$$

where α_i are coefficients of linear combinations and φ_i are basis functions for $i = 1, 2, \dots, n$.

$$\sum_{i=1}^n \alpha_i \int_{\Omega} \left(\frac{\partial \varphi_i}{\partial x} \frac{\partial v}{\partial x} + \frac{\partial \varphi_i}{\partial y} \frac{\partial v}{\partial y} + \frac{\partial \varphi_i}{\partial z} \frac{\partial v}{\partial z} \right) dx dy dz = \int_{\Omega} f v dx dy dz + \int_{\Gamma_N} h v dS. \quad (4.15)$$

Substituting (4.14) for $V(x, y, z)$ or $W(x, y, z)$ to general weak formulation (4.13) or to model BVPs weak formulations in Sec. 6 and also the basis function φ_j for the test function v for $j = 1, 2, \dots, n$, we get a linear system

$$\mathbf{A} \mathbf{u} = \mathbf{f}, \quad (4.16)$$

where \mathbf{A} is the stiffness matrix

$$\mathbf{A} = \begin{pmatrix} \int_{\Omega} \left(\frac{\partial \varphi_1}{\partial x} \frac{\partial \varphi_1}{\partial x} + \frac{\partial \varphi_1}{\partial y} \frac{\partial \varphi_1}{\partial y} + \frac{\partial \varphi_1}{\partial z} \frac{\partial \varphi_1}{\partial z} \right) dx dy dz & \cdots & \int_{\Omega} \left(\frac{\partial \varphi_1}{\partial x} \frac{\partial \varphi_n}{\partial x} + \frac{\partial \varphi_1}{\partial y} \frac{\partial \varphi_n}{\partial y} + \frac{\partial \varphi_1}{\partial z} \frac{\partial \varphi_n}{\partial z} \right) dx dy dz \\ \vdots & \ddots & \vdots \\ \int_{\Omega} \left(\frac{\partial \varphi_n}{\partial x} \frac{\partial \varphi_1}{\partial x} + \frac{\partial \varphi_n}{\partial y} \frac{\partial \varphi_1}{\partial y} + \frac{\partial \varphi_n}{\partial z} \frac{\partial \varphi_1}{\partial z} \right) dx dy dz & \cdots & \int_{\Omega} \left(\frac{\partial \varphi_n}{\partial x} \frac{\partial \varphi_n}{\partial x} + \frac{\partial \varphi_n}{\partial y} \frac{\partial \varphi_n}{\partial y} + \frac{\partial \varphi_n}{\partial z} \frac{\partial \varphi_n}{\partial z} \right) dx dy dz \end{pmatrix}, \quad (4.17)$$

\mathbf{f} is the right-hand side

$$\mathbf{f} = \begin{pmatrix} \int_{\Omega} f \varphi_1 d\Omega + \int_{\Gamma_N} h \varphi_1 dS \\ \vdots \\ \int_{\Omega} f \varphi_n d\Omega + \int_{\Gamma_N} h \varphi_n dS \end{pmatrix}, \quad (4.18)$$

\mathbf{u} is the solution vector

$$\mathbf{u} = (\alpha_1 \alpha_2 \cdots \alpha_n)^T \quad (4.19)$$

and n is the number of basis functions or nodes. In the finite element analysis the weak solution can be improved in several different ways. In the model problems of this master's thesis h and p convergence (Babuška 1982) is studied. As for h convergence the basis functions for each element are fixed and the maximum radial size of the element h_{max} is approaching zero. For p convergence the mesh is fixed and the order of the shape functions p_{min} is approaching p_{∞} . In the model problems, where the analytic solution u^A is known, we evaluate result using a relative error e_{rel} and absolute error e_{abs} , see (Babuška et al. 1981). Let's say, that \tilde{u}_i for every $i = 1, \dots, n$ is the approximated solution obtained at the node i and u_i^A for $i = 1, \dots, n$ is the analytical solution at the

node i . Then the relative error is given by

$$e_{rel} = \frac{\sqrt{\sum_{i=1}^n (\tilde{u}_i - u_i^A)^2}}{\sqrt{\sum_{i=1}^n (u_i^A)^2}} \quad (4.20)$$

and the absolute error is given by

$$e_{abs} = |\tilde{u}_i - u_i^A|. \quad (4.21)$$

It can be shown, that the error estimate of the Galerkin discretization for elliptic differential equation satisfies the Céa's lemma

$$\|u^A - \tilde{u}_i\| \leq \frac{C}{c} \inf_{v_i \in W^{1,2}} \|u^A - v_i\|, \quad (4.22)$$

where $\frac{C}{c}$ are constants. For h-p finite element method we can also write (Babuška 1970/71)

$$\|u - \tilde{u}_i\|_{L^2(\Omega)} \leq ch^{p+1} \|u\|_{W^{1,p+1}}, \quad (4.23)$$

which means that the convergence rate for the solution itself is $O(h^{p+1})$ as is proven in Babuška (1982). The hp-FEM is based on an optimal combination of h and p methodologies which leads to exponential convergence. The problematics of error estimates of the partial differential equations are much more complex. In this master's thesis the validation of the solution is made using the absolute and relative error, however the aprior and aposterior error estimates will be implemented in the future work.

Chapter 5

Software design

5.1 Overview

For the purpose of the numerical solution the author developed the software in C++ e.g (Stroustrup 2013). The compilation is done using the gcc (g++) compiler version 4.8.4. The software is split into two main parts. The first part represents generation of the finite element mesh. For the allocation of matrices and vectors the GNU Science library was used. The algorithms from the GNU Science library for LU, Cholesky and Singular Value decomposition and finding singular values were also used (Brian 2009). These algorithm are often based on routines from LINPACK and LAPACK libraries. The big advantage of using the GNU Science library is the implementation of the algorithms for linear algebra, where the sparse iterative solvers like generalized minimal residual method (GMRES) are included and can be easily implemented in the future work. Another advantage is also the fact, that GNU Science provides a low-level layer which corresponds directly to the C-language BLAS standard

The second part of the software is the FEM algorithm. The FEM algorithm uses the procedures from Bathe (1995). First, the stiffness matrices and the right-hand sides on each element are composed. After that, the global stiffness matrix and the global right-hand side are assembled. As is discussed in Sec. 5.7 and in Sec. 7 the linear system is solved using various direct methods. The big advantage is that we do not have to deal with error from iterative methods and solve the system precisely, however the time of the computation is higher, so some of the iterative methods like conjugate gradient method or GMRES are also consider in the future work. The solution vector u

represents the potential at each node i . A simplified diagram of the computational process is shown in Fig. 5-1.

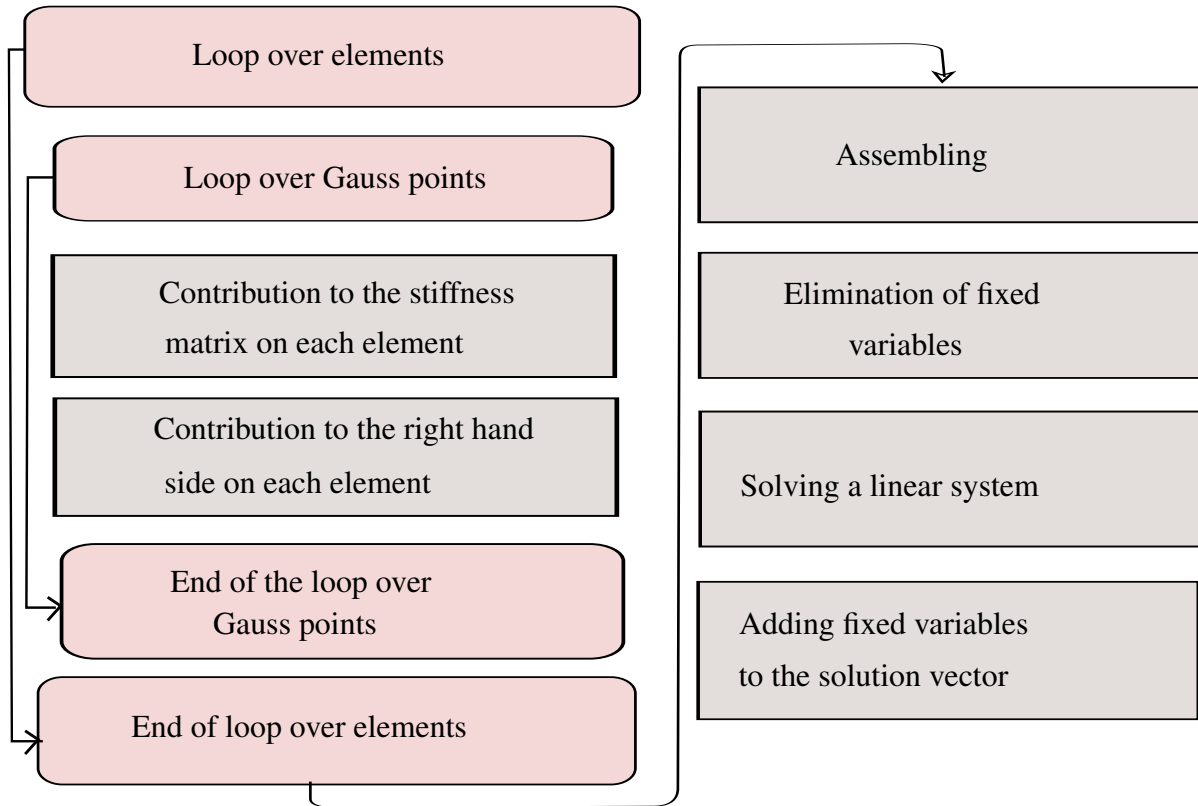


Figure 5-1: Simplified scheme of the potential calculation

5.2 Mesh generation

The finite element mesh is generated using the spherical or ellipsoidal coordinates. Each node is numbered and after the computation the spherical coordinates are transformed to the cartesian coordinates.

$$\begin{aligned}
 x &= \rho \cos \varphi \cos \lambda, \\
 y &= \rho \cos \varphi \sin \lambda, \\
 z &= \rho \sin \varphi.
 \end{aligned}
 \tag{5.1}$$

Then the values of the boundary conditions are assigned to corresponding node. For the boundary value problems of the first category Sec. 6.2.1 the values are computed using the analytical solution (6.2) or (6.5). In contrary, for the global solution the values from the Earth gravitational model (EGM2008) are also used (Pavlis K et al. 2012). When it comes to the global solution, the mesh is much more complex. Therefore the matrix, where the relations of the elements are stored, is also created. From these relations the description matrix (number of nodes for each element) is generated. The input to the FEM algorithm are vectors of cartesian coordinates, description matrix and prescribed values on the boundaries. It is unnecessary, that the order of nodes is the same as in the local coordinates.

5.3 Numerical integration

For the numerical evaluation of the integrals the Gauss-Legendre quadrature with 27 Gauss points on each element for the triple integrals and 9 Gauss points on each side of the element for the surface integrals is used. Denoting the number of Gauss points as NIG , then the numerical integration in three dimensions for general function is performed using the relation

$$\iiint_{\Omega} f(x, y, z) d\Omega = \sum_{i=1}^n w_i \sum_{j=1}^n w_j \sum_{k=1}^n w_k \cdot f(\varphi_g^i, \psi_g^j, \vartheta_g^k), \quad (5.2)$$

where $\varphi_g^i, \psi_g^j, \vartheta_g^k$ is local coordinates of each Gauss point and n is the number of Gauss points on each interval. Analogically for surface integrals the relation is in a form as follows

$$\iint_S f(x, y) dS = \sum_{i=1}^n \sum_{j=1}^n w_j \cdot f(\varphi_g^i, \psi_g^j). \quad (5.3)$$

Each weights can be substituted by the overall weight of each Gauss point

$$\begin{aligned} \sum_{g=1}^{NIG} w_g &= \sum_{i=1}^n w_i \sum_{j=1}^n w_j \sum_{k=1}^n w_k, \\ \sum_{g=1}^{NIG} w_g &= \sum_{i=1}^n w_i \sum_{j=1}^n w_j, \end{aligned} \quad (5.4)$$

and obtain the relations

$$\begin{aligned} \iiint_{\Omega} f(x, y, z) d\Omega &= \sum_{g=1}^{ng} w_g \cdot f(\varphi_g, \psi_g, \vartheta_g), \\ \iint_S f(x, y, z) dS &= \sum_{g=1}^{ng} w_g \cdot f(\varphi_g, \psi_g). \end{aligned} \tag{5.5}$$

The distribution of the Gauss points on each element for the computation of triple integrals is depicted in Fig 5.3. The numerical values of Gauss points coordinates and its weights for Gauss-

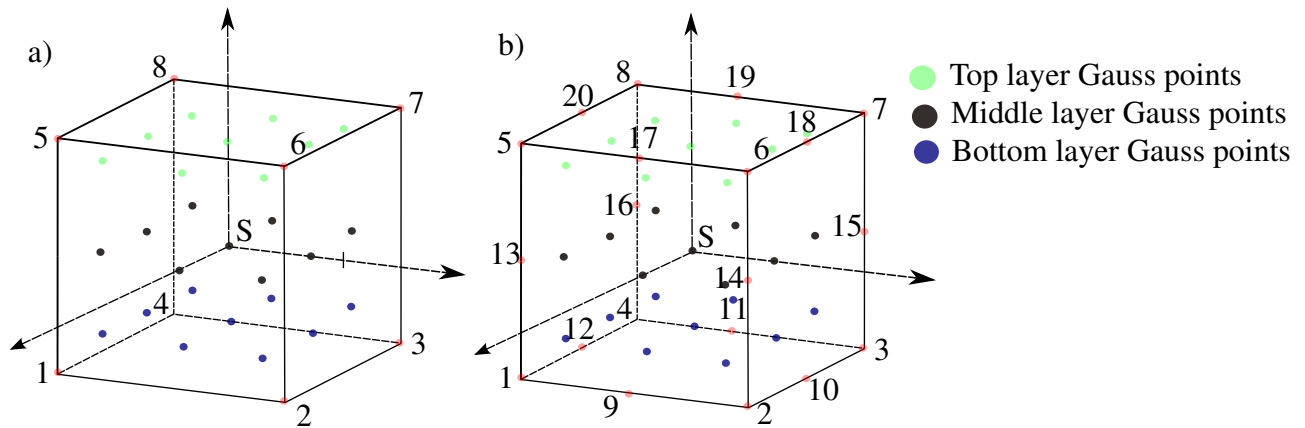


Figure 5-2: Distribution of the Gauss points on each element for the computation of triple integrals in stiffness matrices (5.6)

Legendre quadrature are shown in the Tab 5.1. In the numerical integration in the FEM algorithm the three Gauss points on each interval are used $n = 3$. The element stiffness matrices and the

Table 5.1: Weight of Gauss points

n	Gauss point x_i	Weight of inner Gauss point w_i
1	0	2
2	$\pm\sqrt{\frac{1}{3}}$	1
3	0	$\frac{8}{9}$
	$\pm\sqrt{\frac{3}{5}}$	$\frac{5}{9}$
4	$\pm\sqrt{\frac{(3-2\sqrt{\frac{6}{5}})}{7}}$	$\frac{18+\sqrt{30}}{36}$
	$\pm\sqrt{\frac{(3+2\sqrt{\frac{6}{5}})}{7}}$	$\frac{18-\sqrt{30}}{36}$

right-hand sides are in the form

$$A_e = \iiint_{\Omega_e} \left(\frac{\partial N_i}{\partial x} \frac{\partial N_j}{\partial x} + \frac{\partial N_i}{\partial y} \frac{\partial N_j}{\partial y} + \frac{\partial N_i}{\partial z} \frac{\partial N_j}{\partial z} \right) d\Omega_e, \quad (5.6)$$

$$f_e = \int_{\Omega_e} f N_j d\Omega_e + \int_{\Gamma_N} h N_j d\Omega_e,$$

where N are the shape functions.

5.4 Reference element

In the numerical experiments in this master's these we solve the BVPs with different isoparametric elements, see Fig 4-1. Denote $NELEM$ the number of nodes on each reference element. The first one is 8-noded reference element with linear shape functions. The shape functions for each node are

$$\begin{aligned} N_1 &= \frac{1}{8} (1 - \varphi) (1 - \psi) (1 - \theta), \\ N_2 &= \frac{1}{8} (1 + \varphi) (1 - \psi) (1 - \theta), \\ N_3 &= \frac{1}{8} (1 + \varphi) (1 + \psi) (1 - \theta), \\ N_4 &= \frac{1}{8} (1 - \varphi) (1 + \psi) (1 - \theta), \\ N_5 &= \frac{1}{8} (1 - \varphi) (1 - \psi) (1 + \theta), \\ N_6 &= \frac{1}{8} (1 + \varphi) (1 - \psi) (1 + \theta), \\ N_7 &= \frac{1}{8} (1 + \varphi) (1 + \psi) (1 + \theta), \\ N_8 &= \frac{1}{8} (1 - \varphi) (1 + \psi) (1 + \theta). \end{aligned} \quad (5.7)$$

And the second one is 20-noded reference element with quadratic shape functions

$$\begin{aligned}
N_1 &= \frac{1}{8} (1 - \varphi) (1 - \psi) (1 - \vartheta), \\
N_2 &= \frac{1}{8} (1 + \varphi) (1 - \psi) (1 - \vartheta), \\
N_3 &= \frac{1}{8} (1 + \varphi) (1 + \psi) (1 - \vartheta), \\
N_4 &= \frac{1}{8} (1 - \varphi) (1 + \psi) (1 - \vartheta), \\
N_5 &= \frac{1}{8} (1 - \varphi) (1 - \psi) (1 + \vartheta), \\
N_6 &= \frac{1}{8} (1 + \varphi) (1 - \psi) (1 + \vartheta), \\
N_7 &= \frac{1}{8} (1 + \varphi) (1 + \psi) (1 + \vartheta), \\
N_8 &= \frac{1}{8} (1 - \varphi) (1 + \psi) (1 + \vartheta), \\
N_9 &= \frac{1}{4} (1 - \varphi) (1 + \varphi) (1 - \psi) (1 - \vartheta), \\
N_{10} &= \frac{1}{4} (1 + \varphi) (1 + \psi) (1 - \psi) (1 - \vartheta), \\
N_{11} &= \frac{1}{4} (1 - \varphi) (1 + \varphi) (1 + \psi) (1 - \vartheta), \\
N_{12} &= \frac{1}{4} (1 - \varphi) (1 + \psi) (1 - \psi) (1 - \vartheta), \\
N_{13} &= \frac{1}{4} (1 - \varphi) (1 - \psi) (1 - \vartheta) (1 + \vartheta), \\
N_{14} &= \frac{1}{4} (1 + \varphi) (1 - \psi) (1 - \vartheta) (1 + \vartheta), \\
N_{15} &= \frac{1}{4} (1 + \varphi) (1 + \psi) (1 - \vartheta) (1 + \vartheta), \\
N_{16} &= \frac{1}{4} (1 - \varphi) (1 + \psi) (1 - \vartheta) (1 + \vartheta), \\
N_{17} &= \frac{1}{4} (1 - \varphi) (1 + \varphi) (1 - \psi) (1 + \vartheta), \\
N_{18} &= \frac{1}{4} (1 + \varphi) (1 + \psi) (1 - \psi) (1 + \vartheta), \\
N_{19} &= \frac{1}{4} (1 - \varphi) (1 + \varphi) (1 + \psi) (1 + \vartheta), \\
N_{20} &= \frac{1}{4} (1 - \varphi) (1 + \psi) (1 - \psi) (1 + \vartheta).
\end{aligned} \tag{5.8}$$

In the second case the shape functions in corner nodes 1-8 has to be corrected, so that the shape functions are connected to other shape functions. Relations of these corrections are

$$\begin{aligned}
N_1 &= N_1 - \frac{1}{2}(N_9 + N_{12} + N_{13}), \\
N_2 &= N_2 - \frac{1}{2}(N_9 + N_{10} + N_{14}), \\
N_3 &= N_3 - \frac{1}{2}(N_{10} + N_{15} + N_{11}), \\
N_4 &= N_4 - \frac{1}{2}(N_{12} + N_{16} + N_{11}), \\
N_5 &= N_5 - \frac{1}{2}(N_{13} + N_{20} + N_{17}), \\
N_6 &= N_6 - \frac{1}{2}(N_{17} + N_{18} + N_{14}), \\
N_7 &= N_7 - \frac{1}{2}(N_{19} + N_{18} + N_{15}), \\
N_8 &= N_8 - \frac{1}{2}(N_{16} + N_{20} + N_{19}).
\end{aligned} \tag{5.9}$$

Shape functions are chosen in a way, that value of the shape function at assigned node is 1 and 0 at each other node. For every shape function are also computed its partial derivatives $\frac{\partial N_i}{\partial \varphi}$, $\frac{\partial N_i}{\partial \psi}$, $\frac{\partial N_i}{\partial \vartheta}$, where $i = 1, 2, \dots, NELEM$.

5.5 Mapping the reference element to global coordinates

Now denote global coordinates as x, y, z . General function for mapping can be expressed as

$$\Phi = (x(\varphi, \psi, \vartheta), y(\varphi, \psi, \vartheta), z(\varphi, \psi, \vartheta)), \tag{5.10}$$

Element stiffness matrices A_e are given by

$$\begin{aligned}
A_e = \iiint_{\Omega_e} & \left(\frac{\partial N_i(\varphi_g, \psi_g, \vartheta_g)}{\partial x} \frac{\partial N_j(\varphi_g, \psi_g, \vartheta_g)}{\partial x} + \frac{\partial N_i(\varphi_g, \psi_g, \vartheta_g)}{\partial y} \frac{\partial N_j(\varphi_g, \psi_g, \vartheta_g)}{\partial y} + \right. \\
& \left. + \frac{\partial N_i(\varphi_g, \psi_g, \vartheta_g)}{\partial z} \frac{\partial N_j(\varphi_g, \psi_g, \vartheta_g)}{\partial z} \right) |J_{\Phi}(\varphi_g, \psi_g, \vartheta_g)| d\varphi d\psi d\vartheta
\end{aligned} \tag{5.11}$$

and element right-hand side f_e

$$f_e = \int_{\Omega_e} f N_j |J_{\Phi}(\varphi_g, \psi_g, \vartheta_g)| d\varphi d\psi d\vartheta, \quad (5.12)$$

where $J_{\Phi}(\varphi, \psi, \vartheta)$ is Jacobian in a form

$$J_{\Phi}(\varphi, \psi, \vartheta) = \begin{vmatrix} \frac{\partial x(\varphi, \psi, \vartheta)}{\partial \varphi} & \frac{\partial x(\varphi, \psi, \vartheta)}{\partial \psi} & \frac{\partial x(\varphi, \psi, \vartheta)}{\partial \vartheta} \\ \frac{\partial y(\varphi, \psi, \vartheta)}{\partial \varphi} & \frac{\partial y(\varphi, \psi, \vartheta)}{\partial \psi} & \frac{\partial y(\varphi, \psi, \vartheta)}{\partial \vartheta} \\ \frac{\partial z(\varphi, \psi, \vartheta)}{\partial \varphi} & \frac{\partial z(\varphi, \psi, \vartheta)}{\partial \psi} & \frac{\partial z(\varphi, \psi, \vartheta)}{\partial \vartheta} \end{vmatrix}. \quad (5.13)$$

Members of Jacobian matrix can be computed using derivatives of the shape functions with respect to local coordinates

$$\begin{aligned} \frac{\partial x}{\partial \varphi} &= \sum_{i=1}^{NELEM} x_i \frac{\partial N}{\partial \varphi}, & \frac{\partial y}{\partial \varphi} &= \sum_{i=1}^{NELEM} y_i \frac{\partial N}{\partial \varphi}, & \frac{\partial z}{\partial \varphi} &= \sum_{i=1}^{NELEM} z_i \frac{\partial N}{\partial \varphi}, \\ \frac{\partial x}{\partial \psi} &= \sum_{i=1}^{NELEM} x_i \frac{\partial N}{\partial \psi}, & \frac{\partial y}{\partial \psi} &= \sum_{i=1}^{NELEM} y_i \frac{\partial N}{\partial \psi}, & \frac{\partial z}{\partial \psi} &= \sum_{i=1}^{NELEM} z_i \frac{\partial N}{\partial \psi}, \\ \frac{\partial x}{\partial \vartheta} &= \sum_{i=1}^{NELEM} x_i \frac{\partial N}{\partial \vartheta}, & \frac{\partial y}{\partial \vartheta} &= \sum_{i=1}^{NELEM} y_i \frac{\partial N}{\partial \vartheta}, & \frac{\partial z}{\partial \vartheta} &= \sum_{i=1}^{NELEM} z_i \frac{\partial N}{\partial \vartheta}. \end{aligned} \quad (5.14)$$

Derivatives of the shape functions with respect to global coordinates $\frac{\partial N_i}{\partial x}, \frac{\partial N_i}{\partial y}, \frac{\partial N_i}{\partial z}$ can be computed from the system of linear equations

$$\begin{aligned} \frac{\partial N_i(x(\varphi, \psi, \vartheta), y(\varphi, \psi, \vartheta), z(\varphi, \psi, \vartheta))}{\partial \varphi} &= \frac{\partial N_i}{\partial x} \frac{\partial x}{\partial \varphi} + \frac{\partial N_i}{\partial y} \frac{\partial y}{\partial \varphi} + \frac{\partial N_i}{\partial z} \frac{\partial z}{\partial \varphi}, \\ \frac{\partial N_i(x(\varphi, \psi, \vartheta), y(\varphi, \psi, \vartheta), z(\varphi, \psi, \vartheta))}{\partial \psi} &= \frac{\partial N_i}{\partial x} \frac{\partial x}{\partial \psi} + \frac{\partial N_i}{\partial y} \frac{\partial y}{\partial \psi} + \frac{\partial N_i}{\partial z} \frac{\partial z}{\partial \psi}, \\ \frac{\partial N_i(x(\varphi, \psi, \vartheta), y(\varphi, \psi, \vartheta), z(\varphi, \psi, \vartheta))}{\partial \vartheta} &= \frac{\partial N_i}{\partial x} \frac{\partial x}{\partial \vartheta} + \frac{\partial N_i}{\partial y} \frac{\partial y}{\partial \vartheta} + \frac{\partial N_i}{\partial z} \frac{\partial z}{\partial \vartheta}. \end{aligned} \quad (5.15)$$

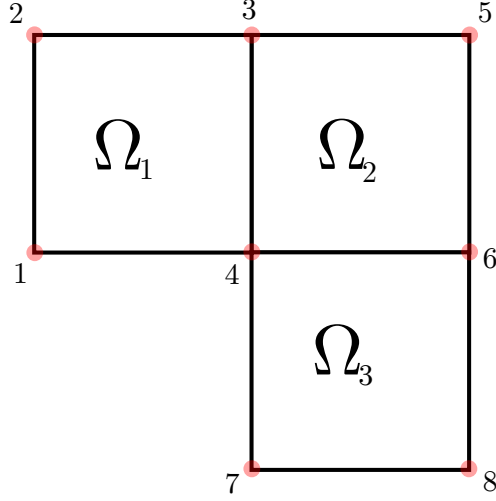


Figure 5-3: Mesh for model example

The global coordinates of each Gauss point can be also computed using these relations

$$\begin{aligned}
 x_g &= \sum_{i=1}^{NELEM} x_i N_i(\varphi_g, \psi_g, \vartheta_g), \\
 y_g &= \sum_{i=1}^{NELEM} y_i N_i(\varphi_g, \psi_g, \vartheta_g), \\
 z_g &= \sum_{i=1}^{NELEM} z_i N_i(\varphi_g, \psi_g, \vartheta_g).
 \end{aligned} \tag{5.16}$$

Finally we can compute contribution to the element stiffness matrix for each node

$$\begin{aligned}
 A_e \approx \sum_{g=1}^{NIG} \omega_g \left(\frac{\partial N_i(\varphi_g, \psi_g, \vartheta_g)}{\partial x} \frac{\partial N_j(\varphi_g, \psi_g, \vartheta_g)}{\partial x} + \frac{\partial N_i(\varphi_g, \psi_g, \vartheta_g)}{\partial y} \frac{\partial N_j(\varphi_g, \psi_g, \vartheta_g)}{\partial y} + \right. \\
 \left. + \frac{\partial N_i(\varphi_g, \psi_g, \vartheta_g)}{\partial z} \frac{\partial N_j(\varphi_g, \psi_g, \vartheta_g)}{\partial z} \right) |J_{\Phi}(\varphi_g, \psi_g, \vartheta_g)|,
 \end{aligned} \tag{5.17}$$

and also the contribution to the right-hand side

$$f_e = \sum_{g=1}^{NIG} w_g f(x_g, y_g, z_g) N_j(\varphi_g, \psi_g, \vartheta_g) |J_{\Phi}(\varphi_g, \psi_g, \vartheta_g)|. \tag{5.18}$$

5.6 Assembling

The process of the global stiffness matrix composition and the right-hand side is demonstrated on the basic example with three elements. The simple mesh for these elements with the numbering are depicted in Fig. 5-3. In the assembling example we denote A_1, A_2, A_3 and the right-hand sides as f_1, f_2, f_3

$$\begin{aligned}
 A_1 &= \begin{pmatrix} a_{11} & a_{12} & a_{13} & a_{14} \\ a_{21} & a_{22} & a_{23} & a_{24} \\ a_{31} & a_{32} & a_{33} & a_{34} \\ a_{41} & a_{42} & a_{43} & a_{44} \end{pmatrix}, & f_1 &= \begin{pmatrix} f_{11} \\ f_{12} \\ f_{13} \\ f_{14} \end{pmatrix}, \\
 A_2 &= \begin{pmatrix} b_{33} & b_{34} & b_{35} & b_{36} \\ b_{43} & b_{44} & b_{45} & b_{46} \\ b_{53} & b_{54} & b_{55} & b_{56} \\ b_{63} & b_{64} & b_{65} & b_{66} \end{pmatrix}, & f_2 &= \begin{pmatrix} f_{23} \\ f_{24} \\ f_{25} \\ f_{26} \end{pmatrix}, \\
 A_3 &= \begin{pmatrix} c_{44} & c_{46} & c_{47} & c_{48} \\ c_{64} & c_{66} & c_{67} & c_{68} \\ c_{74} & c_{76} & c_{77} & c_{78} \\ c_{84} & c_{86} & c_{87} & c_{88} \end{pmatrix}, & f_3 &= \begin{pmatrix} f_{34} \\ f_{36} \\ f_{37} \\ f_{38} \end{pmatrix}.
 \end{aligned} \tag{5.19}$$

Indexes of each element stiffness matrices are assigned according to the finite element mesh (5-3). The basic principle of the assembling process is in addition of the matrix member. In global stiffness matrix are adding these matrix members, which belong to nodes which are on the same

element boundary. Base on this principle we obtain the global stiffness matrix

$$A = \begin{pmatrix} a_{11} & a_{12} & a_{13} & a_{14} & 0 & 0 & 0 & 0 \\ a_{21} & a_{22} & a_{23} & a_{24} & 0 & 0 & 0 & 0 \\ a_{31} & a_{32} & a_{33} + b_{33} & a_{34} + b_{34} & b_{35} & b_{36} & 0 & 0 \\ a_{41} & a_{42} & a_{43} + b_{43} & a_{44} + b_{44} + c_{44} & b_{45} & b_{46} + c_{46} & c_{47} & c_{48} \\ 0 & 0 & b_{53} & b_{54} & b_{55} & b_{56} & 0 & 0 \\ 0 & 0 & b_{63} & b_{64} + c_{64} & b_{65} & b_{66} + c_{66} & c_{67} & c_{68} \\ 0 & 0 & 0 & c_{74} & 0 & c_{76} & c_{77} & c_{78} \\ 0 & 0 & 0 & c_{84} & 0 & c_{86} & c_{87} & c_{88} \end{pmatrix}. \quad (5.20)$$

And the right-hand side

$$f = \begin{pmatrix} f_{11} \\ f_{12} \\ f_{13} + f_{23} \\ f_{14} + f_{24} + f_{34} \\ f_{25} \\ f_{26} + f_{36} \\ f_{37} \\ f_{38} \end{pmatrix}. \quad (5.21)$$

With the solution vector

$$u = \begin{pmatrix} \alpha_1 \\ \alpha_2 \\ \vdots \\ \alpha_8 \end{pmatrix}. \quad (5.22)$$

The system of linear equations are then in a form

$$\begin{pmatrix} a_{11} & a_{12} & \cdots & a_{1n} \\ a_{21} & a_{22} & \cdots & a_{2n} \\ \vdots & \vdots & \ddots & \vdots \\ a_{n1} & a_{n2} & \cdots & a_{nn} \end{pmatrix} \begin{pmatrix} \alpha_1 \\ \alpha_2 \\ \vdots \\ \alpha_n \end{pmatrix} = \begin{pmatrix} f_1 \\ f_2 \\ \vdots \\ f_n \end{pmatrix}. \quad (5.23)$$

or

$$Au = f. \quad (5.24)$$

However we cannot solve the global linear system directly. First, we have to eliminate fixed variables. Denote variables with index *fix*, where the dirichlet condition is assigned, we obtain for example

$$\begin{pmatrix} a_{11} & a_{12}^{fix} & \cdots & a_{1n} \\ a_{21}^{fix} & a_{22}^{fix} & \cdots & a_{2n}^{fix} \\ \vdots & \vdots & \ddots & \vdots \\ a_{n1} & a_{n3}^{fix} & \cdots & a_{nn} \end{pmatrix} \begin{pmatrix} \alpha_1 \\ \alpha_2^{fix} \\ \vdots \\ \alpha_n \end{pmatrix} = \begin{pmatrix} f_1 \\ f_2^{fix} \\ \vdots \\ f_n \end{pmatrix}. \quad (5.25)$$

After elimination we get

$$\begin{pmatrix} a_{11} & a_{13} & \cdots & a_{1n} \\ a_{31} & a_{33} & \cdots & a_{3n} \\ \vdots & \vdots & \ddots & \vdots \\ a_{n1} & a_{n3} & \cdots & a_{nn} \end{pmatrix} \begin{pmatrix} \alpha_1 \\ \alpha_3 \\ \vdots \\ \alpha_n \end{pmatrix} = \begin{pmatrix} f_1 - \alpha_2^{fix} a_{12}^{fix} \\ f_3 - \alpha_2^{fix} a_{32}^{fix} \\ \vdots \\ f_n - \alpha_2^{fix} a_{n2}^{fix} \end{pmatrix}. \quad (5.26)$$

Now we can solve the linear system with various methods, see Sec. 5.7

$$u = \begin{pmatrix} \alpha_1 \\ \alpha_3 \\ \vdots \\ \alpha_n \end{pmatrix}. \quad (5.27)$$

However the solution vector is not complete, so it is necessary to add fixed variable back to the solution vector

$$u = \begin{pmatrix} \alpha_1 \\ \alpha_2^{fix} \\ \alpha_3 \\ \vdots \\ \alpha_n \end{pmatrix}. \quad (5.28)$$

5.7 Solving linear system

First the condition number of the stiffness matrix is computed. For the normal matrices the condition number with respect to L^2 norm is given by

$$\kappa(A) = \|A\| \cdot \|A^{-1}\| = \frac{|\lambda_{max}(A)|}{|\lambda_{min}(A)|} \geq 1, \quad (5.29)$$

where $\lambda_{max}(A)$ is maximal eigenvalue of the matrix A and $\lambda_{min}(A)$ is minimal eigenvalue of the matrix A . The eigenvalues were computed using the GNU Scientific library. The library uses symmetric bidiagonalization and QR reduction method. In order to study convergence precisely it is more sufficient to solve the system accurately with the direct methods, where the error from iterations can be avoided. The brief overview of used direct methods is mentioned in this chapter, nevertheless the more detail view on the methods can be found in Golub et al. (1996) and LAPACK (1999). First we discuss the LU decomposition.

LU decomposition or LU factorization creates a matrix as the product of a lower triangular matrix and an upper triangular matrix. In our case the product includes permutation matrix as well. The LU decomposition can be also viewed as the matrix form of Gaussian elimination and can be used for square systems of linear equations. In the algorithm in the FEM software the LU factorization with partial pivoting is used. This can be written in a form

$$PA = LU, \quad (5.30)$$

where P is permutation matrix, L is unit lower triangular matrix and U is upper triangular matrix. After decomposition we solve the system

$$Ly = Pf \quad (5.31)$$

for y . And use the y vector to obtain the solution u

$$Uu = y. \quad (5.32)$$

A symmetric, positive definite square matrix A has also Cholesky decomposition into a product of

a lower triangular matrix L and its transpose L^T

$$A = LL^T. \quad (5.33)$$

The Cholesky decomposition can only be applied when all the eigenvalues of the matrix are positive, which is satisfied in our case. First the system with y vector is solved

$$Ly = f. \quad (5.34)$$

After that we obtain the solution vector u from the system

$$L^T u = y. \quad (5.35)$$

A general rectangular M -by- N matrix A has a singular value decomposition (SVD) into the product of an M -by- N orthogonal matrix U , an N -by- N diagonal matrix of singular values S and the transpose of an N -by- N orthogonal square matrix V ,

$$A = USV^T. \quad (5.36)$$

Chapter 6

Numerical experiments

6.1 Overview

The numerical experiments in this master's thesis are divided into two main categories. In each model BVPs the Earth's surface is represented by a sphere. The first category are the model boundary value problems, where the convergence of the h-p finite element method is studied. The bottom boundary is in these cases in a shape of spherical trapezoid, see Fig. 6-1. The second category of the numerical experiments are different versions of the fixed geodetic boundary value problem for gravity potential (3.9). In these experiments the methodologies for increasing convergence rate, which have been found using the numerical experiments from the first category, are applied. In these cases the domain is defined as a space between two concentric spheres with radius ρ_{SURF} and ρ_{TOP} , see Fig. 6-2.

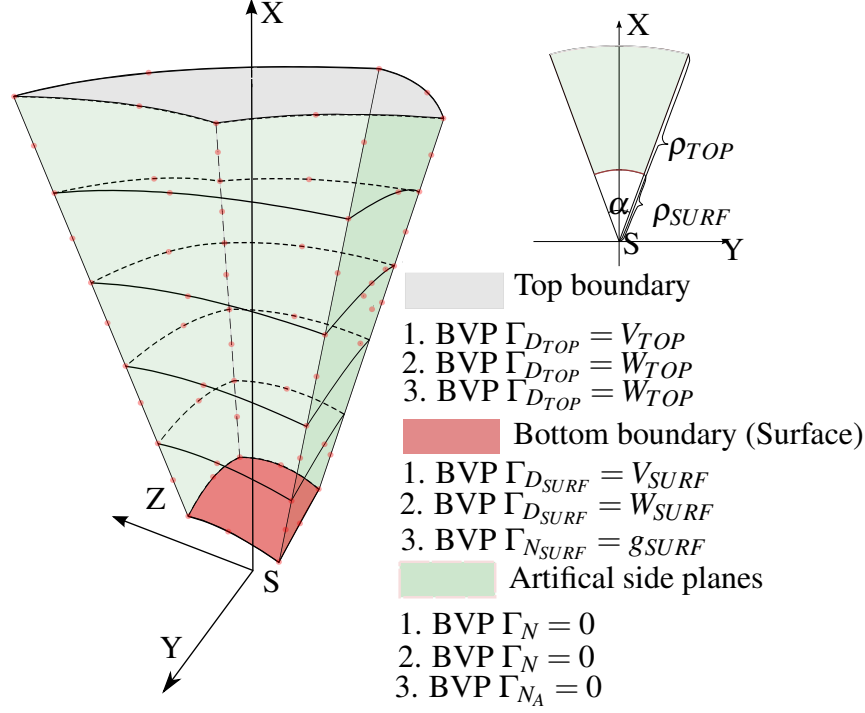


Figure 6-1: Finite element mesh for the first category BVPs with quadratic shape functions and depicted boundary conditions

6.2 Formulations of boundary value problems from the first category

6.2.1 First problem

In the first case the boundary value problem for the gravitational potential $V(x, y, z)$ with the Robin boundary conditions (2.20) is solved. The problem leads to the Laplace's equation, see (3.1)

$$\left(\frac{\partial^2 V}{\partial x^2} + \frac{\partial^2 V}{\partial y^2} + \frac{\partial^2 V}{\partial z^2} \right) = 0. \quad (6.1)$$

The shape of the domain is in a spherical trapezoid shape. The Earth is represented by a sphere with the radius ρ_{SURF} equal to the mean radius of the Earth, see Tab. 6.1. On the Earth's surface and also on the top boundary the Dirichlet conditions have been chosen. The Dirichlet condition on the top boundary is prescribed as V_{TOP} . On the artificial boundaries Γ_{N_A} the Neumann conditions are prescribed as zero, see Fig. 6-1. The analytic solution for the gravitational potential of the

spherically symmetrical body is

$$V(x,y,z) = \frac{GM_{\oplus}}{\rho}, \quad (6.2)$$

where GM_{\oplus} is the standard gravitational parametr for the Earth, see Tab. 2.1. For the purpose of studying convergence of the method the conditions have been chosen constant and the values have been calculated from the relation 6.2. Considering (4.13), we get the weak formulation for the BVP

$$\int_{\Omega} \left(\frac{\partial V}{\partial x} \frac{\partial v}{\partial x} + \frac{\partial V}{\partial y} \frac{\partial v}{\partial y} + \frac{\partial V}{\partial z} \frac{\partial v}{\partial z} \right) dx dy dz = 0. \quad (6.3)$$

The discretization is made using the reference element with quadratic and linear shape functions, see Sec. 4.

6.2.2 Second problem

In the second case the BVP for the gravity potential W . This problem leads to the Poisson's equation, where the Laplacian is equal to $2\omega^2$. Using the general form (4.5), we get

$$\left(\frac{\partial^2 W}{\partial x^2} + \frac{\partial^2 W}{\partial y^2} + \frac{\partial^2 W}{\partial z^2} \right) = 2\omega^2. \quad (6.4)$$

Choosing the analogical boundary conditions as in the first case, we prescribe the Dirichlet condition as W_{SURF} for the bottom boundary and W_{TOP} for the top boundary. However the analytic solution for spherically symmetrical body is now

$$W(x,y,z) = \frac{GM_{\oplus}}{\rho} + \frac{1}{2}\omega^2\rho^2 \cos \varphi. \quad (6.5)$$

Parametr	Value	Units
ρ_{SURF}	6 371 000	[m]
ρ_{SAT}	6 671 000	[m]
ρ_{DEMO}	10^9	[m]
ρ_{∞}	10^{17}	[m]
α	$\frac{\pi}{180}$	[rad]
Longitude λ	$\langle -\alpha; \alpha \rangle$	[rad]
Lattitude φ	$\langle -\alpha; \alpha \rangle$	[rad]
ρ_{THR}	0.55×10^8	[m]

Table 6.1: Parameters for the domain Ω

The Neumann boundary conditions are again equal to zero from the definition of the equipotential surface for the spherically symmetrical body. In the analogical way as in the first case, we obtain the weak formulation

$$\begin{aligned} \int_{\Omega} \left(\frac{\partial W}{\partial x} \frac{\partial v}{\partial x} + \frac{\partial W}{\partial y} \frac{\partial v}{\partial y} + \frac{\partial W}{\partial z} \frac{\partial v}{\partial z} \right) dx dy dz = \\ = \int_{\Omega} 2\omega^2 v d\Omega. \end{aligned} \quad (6.6)$$

The discretization was again made with the reference element with quadratic and linear shape functions.

6.2.3 Third problem

In the third case the BVP is also based on solving Poisson's equation (6.9), but the boundary conditions were chosen in a way, that the model BVP is more similar to the fixed GBVP for gravity potential, see Sec. 3.9. Instead of using the Dirichlet condition W_{SURF} , we prescribe the Neumann condition on the bottom boundary as the magnitude of the gravity vector, see Sec. 3.1

$$g = |\mathbf{g}| = |\mathbf{grad}W|. \quad (6.7)$$

The Neumann boundary Γ_N was split into two boundaries Γ_{N_A} for the artificial sides and $\Gamma_{N_{SURF}}$ for the bottom boundary. The surface integral, which refers to Γ_{N_A} is again equal to zero. The Neumann condition on the Earth's surface was again chosen as constant and calculated from the analytical solution (6.5). The formulation of the BVP is in the form

$$\begin{aligned} \int_{\Omega} \left(\frac{\partial W}{\partial x} \frac{\partial v}{\partial x} + \frac{\partial W}{\partial y} \frac{\partial v}{\partial y} + \frac{\partial W}{\partial z} \frac{\partial v}{\partial z} \right) dx dy dz = \\ = \int_{\Omega} 2\omega^2 v d\Omega + \int_{\Gamma_{N_{SURF}}} |\mathbf{g}| v dS. \end{aligned} \quad (6.8)$$

6.3 Formulations of the boundary value problems of the second category (global solution)

In the numerical experiments from the second category the so-called global solution of the geodetic boundary value problem is solved. The domain is in this case chosen as two concentric spheres with radius ρ_{SURF} and ρ_{TOP} , see Fig. 6-2. Hence we do not have to put boundary conditions on the artificial sides. The boundary conditions are prescribed only on the Earth's surface and on the upper boundary. The fixed geodetic boundary value problem is formulated in Sec. 3.9. This GBVP is formulated by Poisson's equation

$$\left(\frac{\partial^2 W}{\partial x^2} + \frac{\partial^2 W}{\partial y^2} + \frac{\partial^2 W}{\partial z^2} \right) = 2\omega^2. \quad (6.9)$$

On the surface of the Earth is prescribed Neumann condition as magnitude of the gravity acceleration g . On the top boundary is the Dirichlet condition prescribed. The weak formulation is analogical to the (6.8) and is in the form

$$\begin{aligned} \int_{\Omega} \left(\frac{\partial W}{\partial x} \frac{\partial v}{\partial x} + \frac{\partial W}{\partial y} \frac{\partial v}{\partial y} + \frac{\partial W}{\partial z} \frac{\partial v}{\partial z} \right) dx dy dz = \\ = \int_{\Omega} 2\omega^2 v d\Omega + \int_{\Gamma_{NSURF}} |\mathbf{g}| v dS. \end{aligned} \quad (6.10)$$

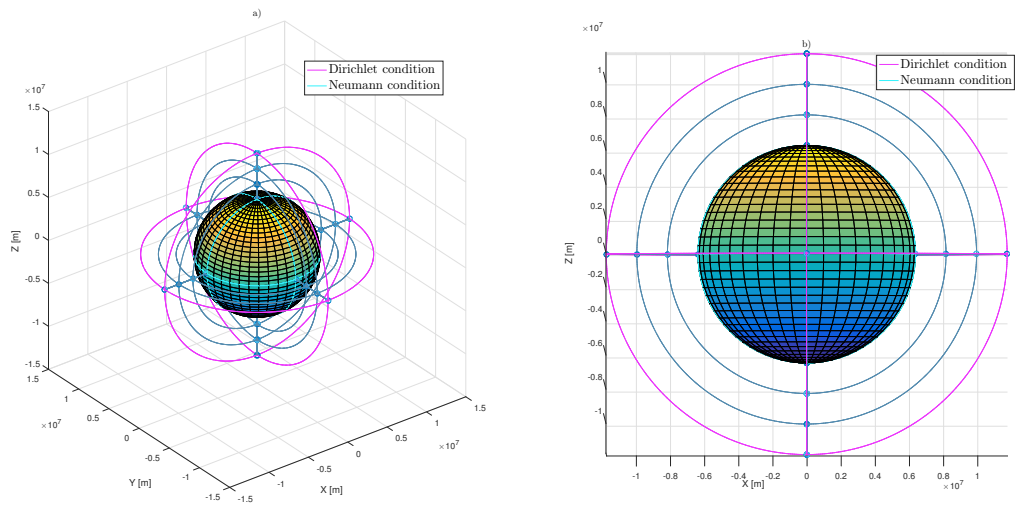


Figure 6-2: Methodology for choosing boundary condition on the simple finite element mesh

Chapter 7

Results

7.1 Solution of the linear system

The number of equations in the linear system is equal to the number of nodes N with the subtraction of the number nodes, where the Dirichlet boundary conditions are assigned. As for the time of the computation, solving the linear system is the biggest concern in the finite element method. The solution of the finite element method mostly leads on the linear system with a sparse banded matrix. The numerical experiments in this master's thesis also lead on the linear system with the symmetrical banded matrix, although the width and the sparcity of the stiffness matrix vary. The number of nodes for the experiments, where the domain is in the shape of spherical trapesoid and discretization is done only in radial direction, is $N = 4NEL + 4$ for the linear shape functions and $N = 12NEL + 8$ for quadratic shape functions. The width of the matrix is equal to 12 for linear shape functions. The structure of the stiffness matrix for the numerical experiment with 30 elements is depicted in Fig. 7-1. When it comes to the stiffness matrix of the global solution, see Fig. 7-8, the stiffness matrix is also banded matrix, however the width is larger and depends on the discretization in terms of λ and φ . The structure of the stiffness matrix is shown in Fig. 7-2. As it was mentioned, all numerical experiments in this thesis lead to banded stiffness matrix. In Sec. 5.7 different direct methods for solution of the linear system were discussed. The algorithms are implemented using the GNU Science library. The Cholesky decomposition exploits the best symmetric band structure of the matrix as is also proofed by the numerical experiments in Tab. 7.1. The elapsed time follows theoretical complexity and as it shown the Cholesky decomposition

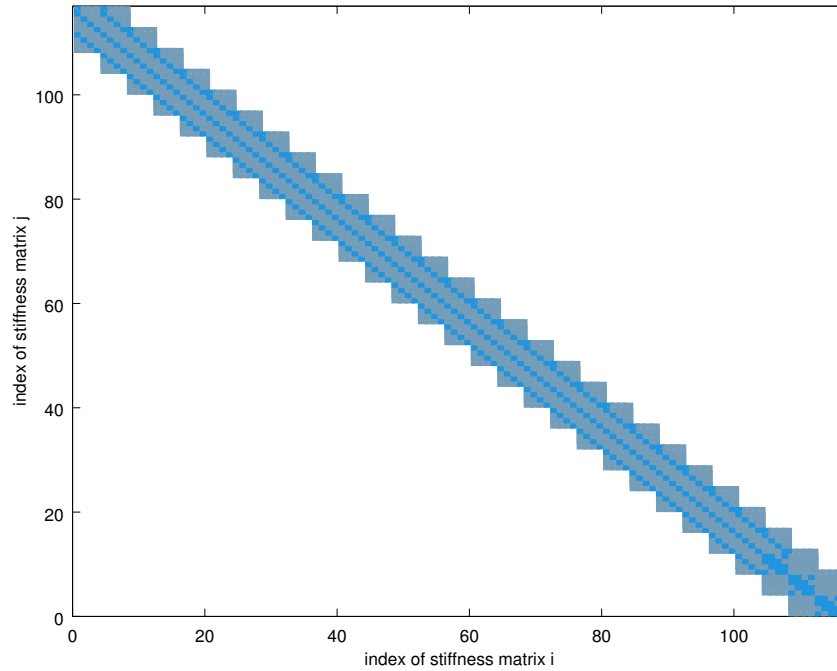


Figure 7-1: The structure of the stiffness matrix for convergence experiments (This example is made for the mesh, where the domain is discretized by thirty elements in radial direction)

is the best also for the global solution, even if the sparsity of the stiffness matrix is lower and the width of the band is higher. All calculation of the numerical experiments were done on Ubuntu 14.04 with the Intel(R) Core(TM) i5-3570k with two 4 GiB Kingston DIMM DDR3 Synchronous with clock 1333 MHz and little endian byte order. As the result of these findings all the numerical experiments in Sec. 7.2 and Sec. 7.3 are solved using the Cholesky decomposition.

Method	3996 eq. (spherical trapesoid)	12012 eq. (global solution)
LU	20s	562.479s
SVD	864s	—
CHOL	10s	266s

Table 7.1: The time elapsed for solving the linear system using the various methods. The domain is discretized by 1000 elements in radial direction.

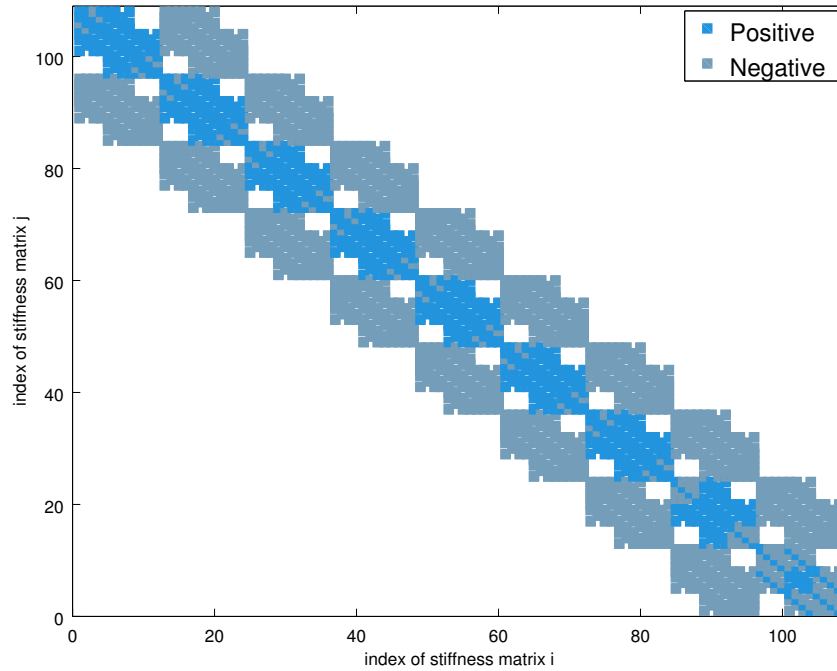


Figure 7-2: The structure of the stiffness matrix for basic example of the global solution, see Fig. 7-8

7.2 Convergence experiments

The convergence numerical experiments are mostly based on the experiments computed in Mráz et al. (2015a;2015b) and Mráz et al. (2016). The convergence experiments are only solved with constant Dirichlet and Neumann condition. The values of these conditions are obtained from the analytical solutions, so that it is possible to compare the weak solution with the analytical solution. Then the results are much more valuable for studying radial convergence and it is also much easier to compute the relative and absolute error. Although the analytical solution is known only for some special cases, we can use the convergence tendencies for solving the real GBVP with the measured or synthetic data, see 7.3.

A geometry of the domain is similar for every numerical experiment. The shape of the domain is defined by the values of the radial distance ρ , the longitude λ and the latitude φ , see Tab. 6.1. The size of the domain for each numerical experiment differs only in the radial direction. The surface of the Earth is represented by a sphere with the mean radius of the Earth, see Tab. 6.1. Upper and lower boundaries are of spherical shape and the rest artificial boundaries are of plane shape, see

Fig. 5-3. For the purpose of studying radial convergence the domain is only discretized in radial direction by NEL elements, where NEL is the number of elements in the domain. Discretization is done by the isoparametric elements with linear or quadratic shape functions (Ergatoudis 1968), see Fig. 4-1. In the first model BVP the Laplace equation (6.1) is solved. The mesh is only discretized in radial direction with 30, 60, 120, 240 and 480 elements. The size of each element in radial direction is constant. The differences between different discretizations and analytical solution are in Fig. 7-3.

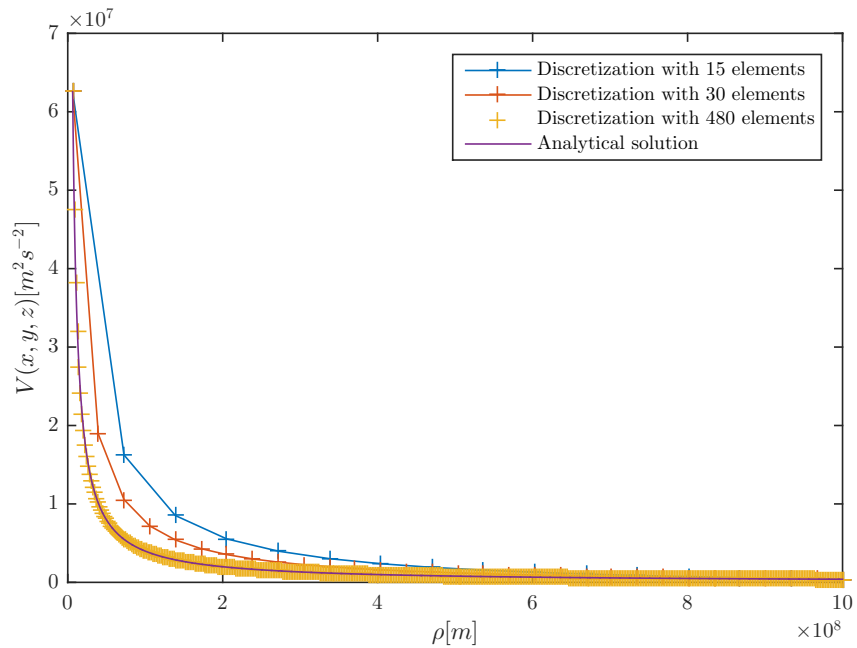


Figure 7-3: Increasing convergence with the h methodology. The linear shape functions are used. The meshes are generated with the constant radial size of each element. The domain is bounded with the top boundary $\rho_{TOP} = \rho_{DEMO}$.

The reference element is 8-noded with linear shape functions, see Fig. 4-1a. Size of the domain in radial direction is bounded by ρ_{SURF} and ρ_{DEMO} . The value V_{TOP} can not be in this height represented by real data, but for the illustrative purpose is computed from the analytical solution (6.2). Nevertheless the h methodology is not the only method for increasing the rate of convergence as it stated in Sec. 4. With p methodology we increase the order of the shape functions. The results for the domain discretized by 5 elements in radial direction with linear and quadratic shape function are shown in Fig. 7-4.

In the first set of meshes the radial size of each element is constant, but the meshes, where the

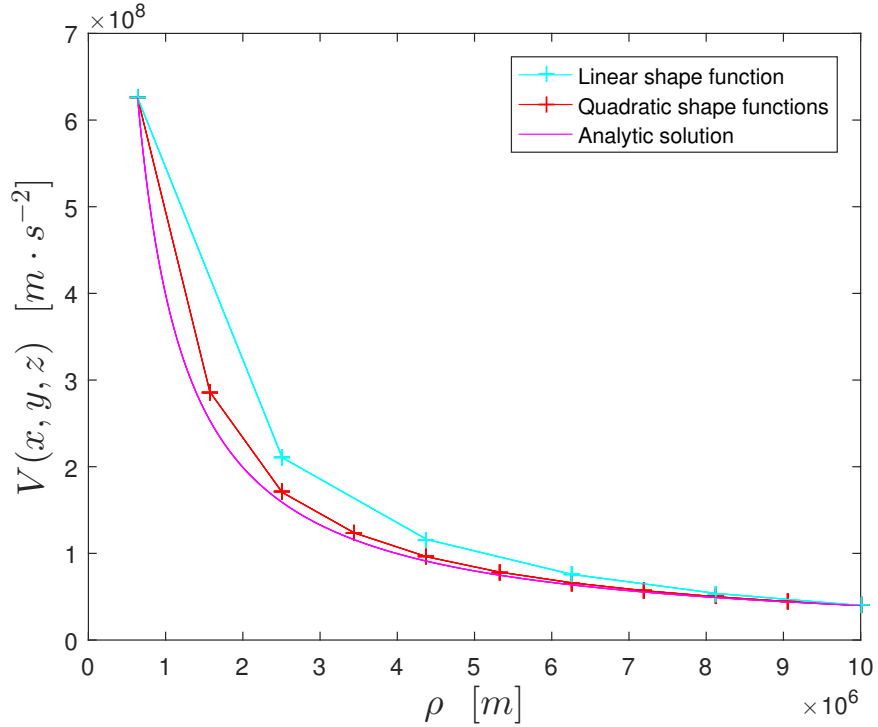


Figure 7-4: Increasing the convergence rate using the p methodology with 5 elements in radial direction with linear and also quadratic shape functions

radial size of the element is dependent on the rate of change of the potential, are also generated. The principle of the mesh generation for the model BVP (6.9) is, that we substitute ρ_{SURF} and ρ_{TOP} into the relation for the magnitude of the gravity acceleration (6.7). From this relation we obtain the values g_{SURF} and g_{TOP} . By these values the interval for radial discretization is defined and we can compute the values

$$g_i = g_{SURF} + i \frac{g_{TOP} - g_{SURF}}{NEL}, \quad (7.1)$$

where $i = 0, \dots, NEL$. By rearranging (6.7) and substituting values g_i into this relation, we obtain the radial distance ρ_i for each nodal point. The relative error e_{rel}^E for the h methodology with the same radial size for each element and the relative error for the h methodology with the mesh generation dependent on the potential change e_{rel}^D is depicted in Fig. 7-5. The numerical values are in Tab. 7.2.

This method of mesh generation is not suitable for the type of the domain, where the radial size

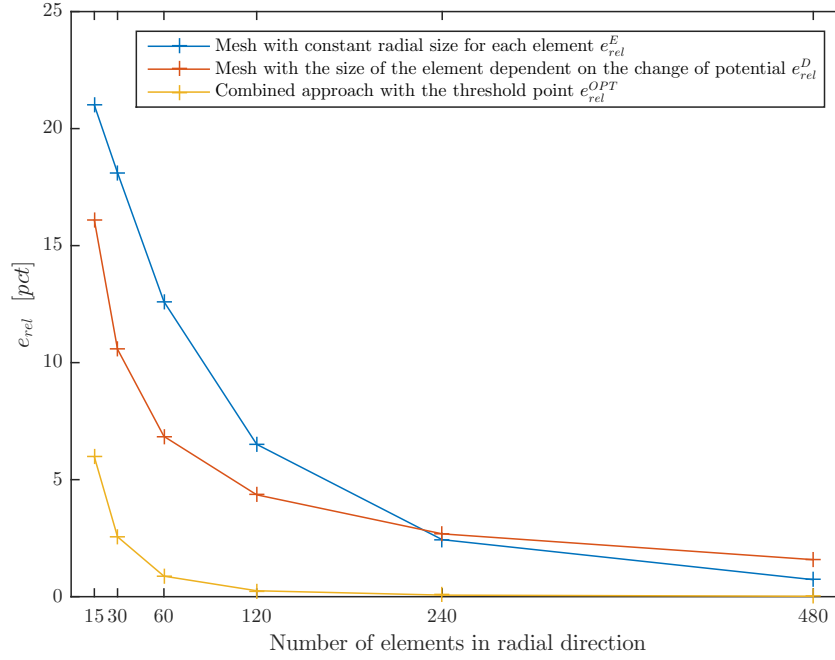


Figure 7-5: The relative error for different mesh generation. The domain is bounded by $\rho_{TOP} = \rho_{DEMO} = 10^9$. In these cases we solve the Laplace equation with the isoparametric reference element with linear shape functions

of the domain is too large, $\rho_{TOP} \geq 10^8$, see Fig. 7-6.

As seen in Fig. 7-7, the better way to generate the mesh is to combine the both approaches. We split the domain into two parts. In the first part, where the rate of change is fast, use the mesh generation with the dependence on the potential change and in the second part generate a mesh with the constant radial size of the element. The threshold point for splitting the domain should be close to the saddle point. It was found, that the best point for splitting the domain is $\rho_{THR} \approx 0.55 \times 10^8$

NEL	e_{rel}^E [pct]	e_{rel}^D [pct]	e_{rel}^{OPT} [pct]
15	21.09	16.09	5.97
30	18.11	10.57	2.56
60	12.61	6.85	0.88
120	6.51	4.35	0.25
240	2.44	2.68	0.066
480	0.73	1.58	0.017

Table 7.2: Relative errors for different mesh generation with the dependence on the number of elements in radial direction

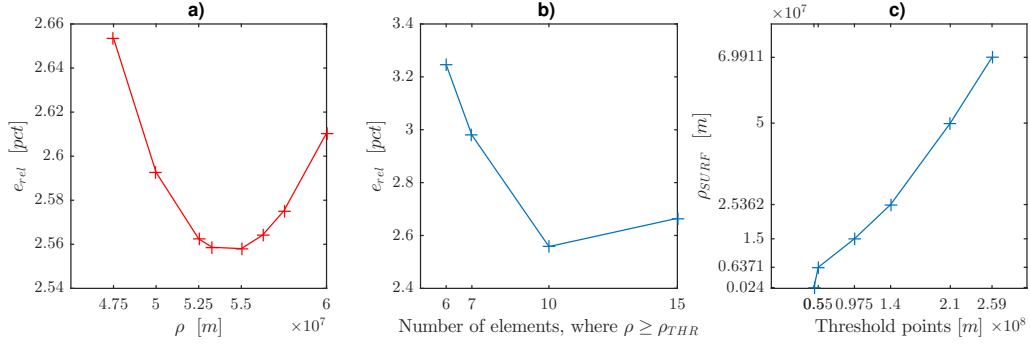


Figure 7-6: a) Finding the threshold point with minimum relative error on the mesh with 30 elements b) Finding the distribution of the elements in radial direction with the minimum relative error on the mesh with 30 elements

and also the distribution of the elements in the ratio $\frac{2}{3}NEL$, where $\rho \leq \rho_{THR}$ and $\frac{1}{3}NEL$, where $\rho \geq \rho_{THR}$, is optimal. These values are found by running a number of numerical experiments for different thresholds and for different distributions of the elements. In these experiments relative error as a determining parameter for choosing optimal threshold and optimal distribution of the elements is used, see Fig. 7-6.

To solve the problem, which is similar to the geodetic boundary value problem, we have to solve the model boundary value problem (6.8), where the input data are equal to magnitude of gravity acceleration g . Absolute errors are depicted in Fig. 4.21.

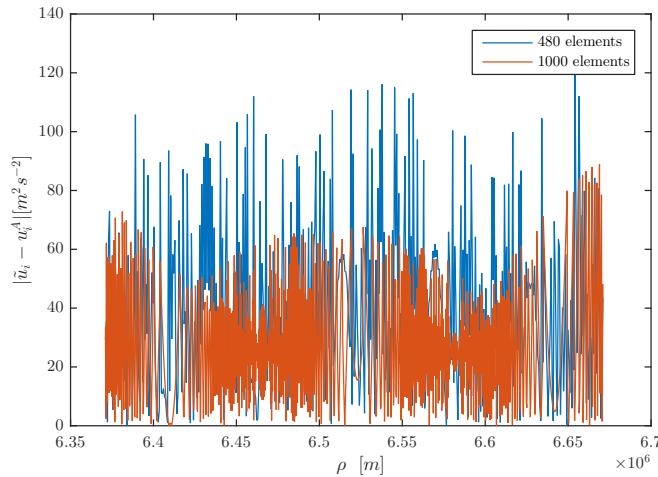


Figure 7-7: The overall absolute differences for the solution of the model BVP in Sec. 6.2.2 with the Dirichlet condition W_{SURF} on the bottom boundary. The domain is in radial direction bounded by ρ_{SURF} and ρ_{SAT} . The mesh was generated with the constant radial size of the element. The isoparametric reference element with linear shape functions is used.

7.3 Global solution

For the purpose of validation of the global solution a simple model problem is solved. The solution demonstrates the principle of the global solution and is depicted in Fig. 7-8. The boundary conditions are constant in this case. On the Earth's surface the Dirichlet condition as gravitational potential is prescribed. The singularities on the poles are modelled in a similar way as in Meissel

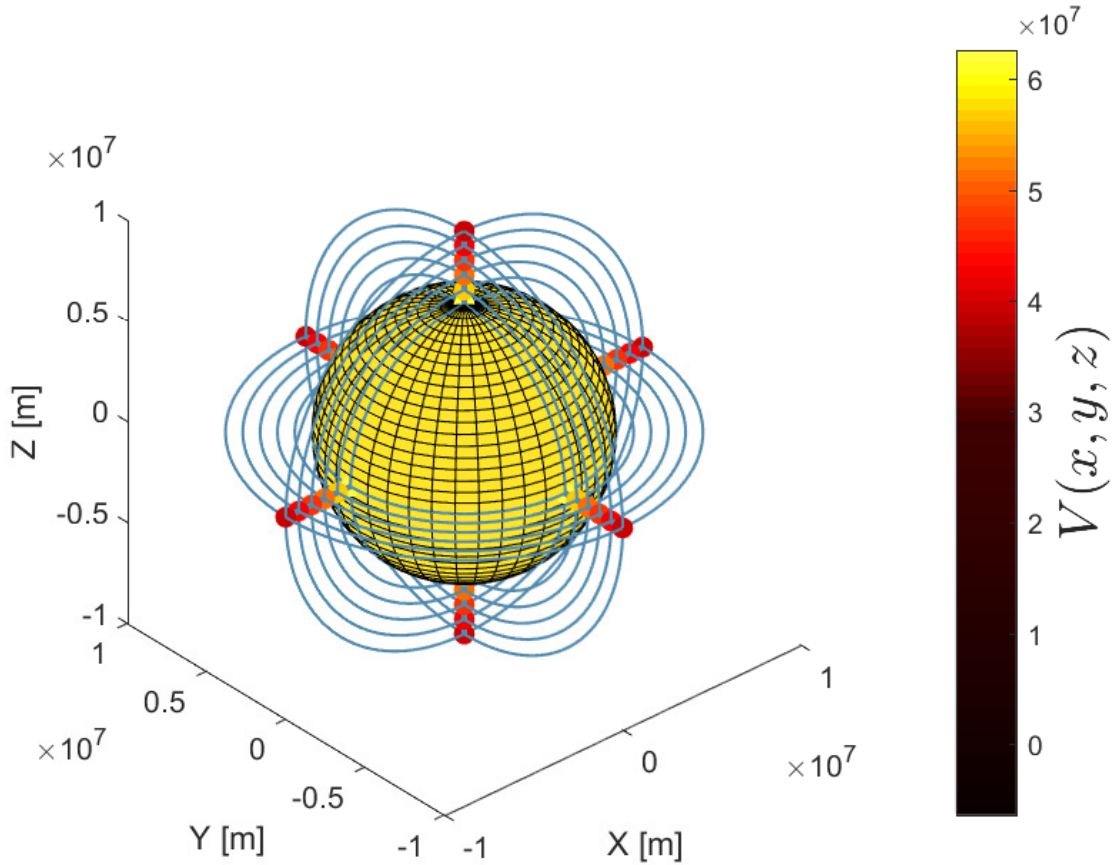


Figure 7-8: Global solution for the gravitational potential V , where the Dirichlet boundary conditions are prescribed on the surface and the top boundary. The domain is discretized by 5 element in terms of radial direction and bounded by $\rho_{TOP} = 10^9$. Reference surface is the sphere with the mean radius of the Earth.

(1981). Detail of the solving the pole singularity is depicted in Fig. 7-9. The part of the domain on the poles is in terms of λ and φ defined by very small angle e.g. $0.0001 [deg]$. As it was expected the potential is constant on each layer. The body has the same property as the point mass and converges to the analytic solution of the spherical symmetrical body. In radial direction the

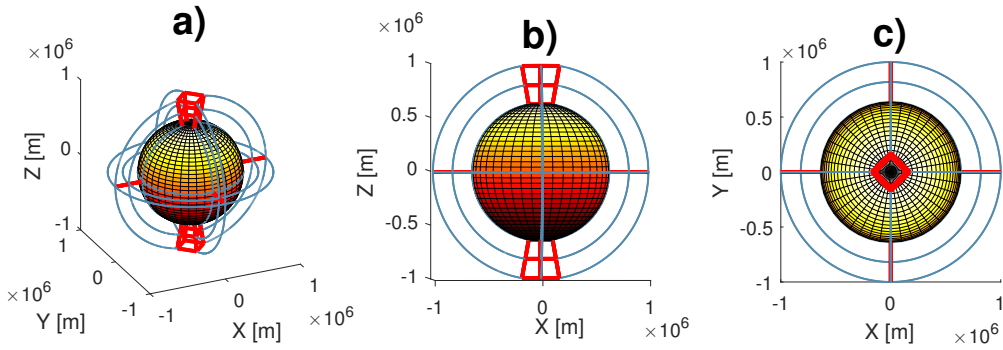


Figure 7-9: Detail on the generating mesh on the poles a) overview b) profile c) perspective. For illustrative purpose the angle, which defines spherical trapesoid in terms of λ and φ , is equal to 20 degrees. However in the computation of the geodetic boundary value problem is the angle equal to 0.0002.

φ [deg]	λ [deg]	Gravity anomaly Δg [mGal]
89.9583333333	0.0416666667	3.25491
89.9583333333	0.1250000000	3.24581
89.9583333333	0.2083333333	3.23676

Table 7.3: Example of the output from the official FORTRAN program

equipotential surface has the same value as it was computed in the model problems, where the convergence was analyzed.

In the second global solution the geodetic boundary value problem, where the data on the surface are obtained from the Earth gravitational model (EGM2008), is solved. The geodetic boundary value problem is discussed in Sec. 3.3 and formulated more precisely in Sec. 6.3. The EGM2008 data are in a form of binary file with small or big endian byte order. The binary files with small endian byte order are used. The data are available in grids $2,5' \times 2,5'$ and $5' \times 5'$. In these binary files the gravity anomalies, deflections of the vertical and geoid undulation at each node of the grid are stored. Example of the output is shown in Tab. 7.3. The geoid undulation are with the respect to WGS84 reference ellipsoid. Parameters for the WGS84 ellipsoid are shown in Tab. 3.2. The magnitude of the gravity vector on the poles and equator are defined by the free-air gravity anomaly (3.14) with the addition of the magnitude of the normal gravity vector, which is calculated from the Somigliana-Pizzetti formula (3.18). As it is previously mentioned the oblique derivative effect was neglected, therefore the deflections of the vertical were not used. Solving the

geodetic boundary value with all the data will lead to large linear system, where the computer with higher computational power has to be used. Therefore the computation of the basic model geodetic boundary value problem was performed.

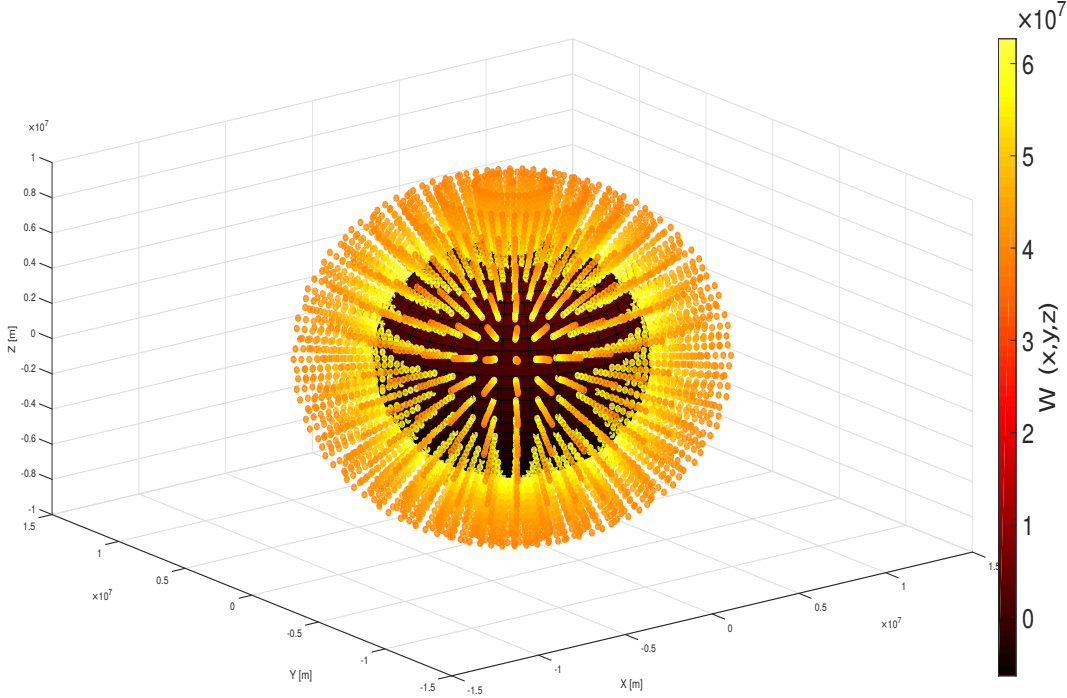


Figure 7-10: Computation of the gravity potential W . The problem is formulated as the geodetic boundary value problem in Sec. 6.3. On the Surface's of the Earth the Neumann condition with the magnitudes of the gravity acceleration g is prescribed. The oblique derivative effect was neglected.

Chapter 8

Conclusion

The main aim of this master's thesis was to study the application of the h-p FEM in the problems of physical geodesy. For that purpose the weak formulations for the model BVPs were derived and the h-p FEM algorithm for solving these model BVPs was implemented by the FEM software written in C++. For the high performance computations the GNU Scientific library with BLAS support is used. Two kinds of numerical experiments have been performed. In the experiments of the first category the rate of convergence of the h-p finite element method in radial direction has been studied. The main goal of these experiments was to study the rate of convergence for h and p methodology and also to find the optimal ways for the mesh generation. In the second kind of the experiments the methodology for the computation of the so-called global solution is researched. A number of numerical experiments with different meshes and differently sized domains has been computed. As is mentioned in Mráz et al. (2016), the best way to generate meshes is to split the domain into two parts. In the first part we can use the mesh generation dependent on the potential change. In the second part we can use the mesh generation with the same radial size for each element.

In order to decide, which methodology to choose, we have to take into account the difficulty of the programming for the p methodology and also the fact, that the computation with the linear shape functions is more efficient. In the case, where the mesh is discretized only in radial direction, the linear system for quadratic shape functions has $12NEL + 8$ equations and only $4NEL + 4$ equations for linear shape functions. In general, the improvement with the p methodology in radial direction is not worth the increased computational power. We can obtain much better results if we

use the h methodology with the mesh generation using the threshold point. If we use this combined approach, the linear system has the same amount of equations as with the h methodology with the constant radial size of the element, but the rate of convergence increases much faster than with the p methodology. However the advantage of using the isoparametric reference element with quadratic shape is in approximating source of the gravitation. These aspects of approximation and application of these methods for modelling terrain deformations will be studied in future. In my opinion is not worth to apply elements with higher order shape functions in the remote zones in terms of radial direction, but it is valid to apply these elements for zone, which are closer to the Earth's surface. For solving the linear system the LU decomposition, Cholesky decomposition and singular value decomposition have been used. In every numerical experiment the stiffness matrix is symmetrical and banded. It has been proven by the numerical experiments, that the most efficient way to directly solve the linear system is to use Cholesky decomposition, which is approximately twice as fast as LU decomposition. Computing the system using the singular value decomposition takes much more time, than with other methods. This was assumed due the theoretical complexity of the algorithm. However the singular value decomposition has its application in the cases, where the distribution of the surface data are in special configurations and the linear system becomes unstable.

The second type of the experiments are the computation of the global solution. The author suggests to apply discussed methodology of the mesh generation for modelling the singularities on the Earth's pole. A few experiments have been performed. In these experiments the gravitational potential and gravity potential using the constant data and the data from the EGM2008 have been computed.

The FEM algorithm and convergence tendencies will be applied for the precise local and global gravity field modelling. I want to also solve not only fixed geodetic boundary value problem for gravity potential W , but also the geodetic boundary value problem for disturbing potential T (fixed gravimetric boundary value problem). The other challenges are to implement a priori and a posteriori error estimates, adaptive mesh refinement, Gauss-Konrod rules for the numerical integration, to solve the geodetic boundary value problem on the supercomputer, apply sufficient algorithm for solving the oblique derivative effect and also to study the effect of the terrain deformations on the weak solution. The results of these efforts can be the set of methodologies and software published

as open source, where the local and global gravity field models can be computed with high resolution. The goal is to compute the geodetic boundary value problem with 1 cm accuracy in terms of computation. Opposed to the classical solution computed using the spherical harmonics, the application of the h-p FEM offers much more genericity. It is more suitable for the areas, where the big changes in terms of gravity are and in my opinion the more precise solution can be also obtained using the right methodologies.

Bibliography

- [1] Adams, Robert A.; Fournier, John (2003) [1975]. Sobolev Spaces. Pure and Applied Mathematics. 140 (2nd ed.). Boston, MA: Academic Press. ISBN 978-0-12-044143-3
- [2] Axelsson O, Barker V (2001) Finite Element Solution of Boundary Value Problems: Theory and Computation. A Society for Industrial and Applied Mathematics
- [3] Babuška I, Dorr M R (1981) Error estimates for the combined h and p version of finite element method. Numer. Math. 37, 252277
- [4] Babuška I, Szabo B (1982) On the rates of convergence of the finite element method. Int. J. Numer. Meth. Engng., 18: 323341. doi:10.1002/nme.1620180302
- [5] Babuška I, Suri M (1990) The p- and h-p versions of the finite element method an overview, in Spectral and High Order Methods for Partial Differential Equations, C. Canuto and A. Quarteroni eds., North-Holland, Amsterdam, pp.5-26
- [6] Babuška I Error-Bounds for Finite Element Method, Numerische Mathematik (1970/71), Volume: 16, page 322-333
- [7] Bathe K (1999) Finite Element Procedures. Prentice Hall
- [8] Bjerhammar A, Svensson L (1983) On the geodetic boundary-value problem for a fixed boundary surface - satellite approach. Bull. Geod., 57: 382-393
- [9] Brian G (2009) GNU Scientific Library Reference Manual - Third Edition
- [10] Čunderlík R, Mikula K, Mojzeš M (2008) Numerical solution of the linearized fixed gravimetric boundary-value problem. J Geod 82(1):1529

- [11] Ergatoudis J, Irons B and Zienkiewicz O (1968) Curved, isoparametric, quadrilateral elements for finite element analysis, *Int. J. Solids Struct.* 4, 31-42
- [12] Evans L C (1998) *Partial Differential Equations*. Providence: American Mathematical Society
- [13] Fašková Z, Čunderlík, Mikula K (2010) Finite element method for solving geodetic boundary value problems. *Journal of Geodesy*, Vol. 84, Issue 2 (2010) pp 135-144
- [14] Grafarend E, Niemeier W (1971) The free nonlinear boundary value problem of physical geodesy. *Bull Geod* 101:243261CrossRef
- [15] Grafarend E (1989) The geoid and the gravimetric boundary value problem, Report No 18. The Royal Institute of Technology (Dep of Geod), Stockholm
- [16] Grafarend E, Heck B, Knickmeyer E (1985) The free versus fixed geodetic boundary value problem for different combinations of geodetic observables. Springer Verlag, *Bull Geod* Vol 59(1):11-32
- [17] Golub G H, Van Loan C F *Matrix Computations (Third Edition)* The Johns Hopkins University Press, Baltimore, MD (1996)
- [18] Heck B (1989) On the non-linear geodetic boundary value problem for a fixed boundary surface. *Bull Geod* 63(1):5767
- [19] Hofmann-Wellenhof B, Moritz H (2005) *Physical Geodesy*. Springer-Verlag, New York
- [20] Holota P and Nesvadba O (2007) Model refinements and numerical solutions of weakly formulated boundary-value problems in physical geodesy. In: Xu P., Liu J. and Dermanis A. (eds.): VI Hotine-Marussi Symp. of Theoretical and Computational Geodesy, Wuhan, China, 29 May - 2 June, 2006. *IAG Symposia*, Vol. 132, Springer, Berlin-Heidelberg-New York, 2007: 314-320
- [21] Holota P (2000) Direct methods in physical geodesy. In: Schwarz K.-P. (ed.). *Geodesy Beyond 2000 - The Challenges of the First Decade*. IAG General Assembly, Birmingham, July 19-30, 1999, *IAG Symposia*, Vol. 121, Springer, Berlin - Heidelberg - New York, 2000: 163-170

- [22] Holota P (2001) Variational methods in geoid determination and function bases. *Phys Chem Earth Solid Earth Geodes* 24(1):3-14
- [23] Holota P (2005) Neumanns boundary-value problem in studies on Earth gravity field: weak solution. In: Holota P. and Slaboch V. (Eds), 50 years of Research Institute of Geodesy, Topography and Cartography, Prague. Research Institute of Geodesy, Topography and Cartography, Vol. 50, No. 36, 4969
- [24] Hormander L (1975) The boundary problems of physical geodesy. The Royal Inst. of Technology, Division of Geodesy, Stockholm, 1975; Mso in: *Archive for Rational Mechanics and Analysis*
- [25] Klees R (1995) Boundary value problems and approximation of integral equations by finite elements. *Manuscripta Geodaetica*, 20, 345-361
- [26] Klees R, van Gelderen M, Lage C and Schwab C (2001) Fast numerical solution of the linearized Molodensky problem. *J. Geodesy*, 75, 349362
- [27] Koch K.R. and Pope A.J. (1972): Uniqueness and existence for the geodetic boundary value problem using the known surface of the Earth. *Bull. G od.* 106, 467-476
- [28] LAPACK Users Guide (Third Edition, 1999), Published by SIAM, ISBN 0-89871-447-8.
- [29] Meissl P (1981) The use of finite elements in physical geodesy. Report 313, Geodetic Science and Surveying, The Ohio State University
- [30] Minarechová Z, Macák M, Čunderlík R, Mikula K (2015) High-resolution global gravity field modelling by the finite volume method. *Stud Geophys Geod* 59(1): 1-20
- [31] Mráz D, Bořík M, Novotný J Application of the finite element method in problems of physical geodesy. In: *Proceedings of IAMG 2015. The 17th annual conference of the International Association for Mathematical Geosciences. Freiberg (Saxony), 05.09.2015 - 13.09.2015. Freiberg: Freiberg University of Mining and Technology, Institute of Computer Science. 2015, s. 665-672. ISBN 978-3-00-050337-5.*

- [32] Mráz D, Bořík M, Novotný J Numerical solution of the geodetic boundary value problem using the finite element method. In: 26th IUGG General Assembly 2015. 26th IUGG General Assembly 2015. Prague, 22.06.2015 - 02.07.2015. 2015, s. 146.
- [33] Mráz D, Bořík M, Novotný J On the Convergence of the h-p Finite Element Method for Solving Boundary Value Problems in Physical Geodesy, Springer Berlin Heidelberg, Berlin, Heidelberg, 10.1007/1345_2016_237,
- [34] Nečas J (2003) Direct Methods in the Theory of Elliptic Equations
- [35] Nesvadba O, Holota P and Klees R (2007) A direct method and its numerical interpretation in the determination of the Earth's gravity field from terrestrial data. In: Tregoning P. and Rizos C. (Eds.), Dynamic Planet. International Association of Geodesy Symposia, 130. SpringerVerlag, Heidelberg, Germany, 370376
- [36] Pavlis K et al. The development and evaluation of the Earth Gravitational Model 2008 (EGM2008) - Journal of Geophysical Research: Solid Earth (1978-2012) Volume 117, Issue B4, April 2012
- [37] Rektorys K (1980) Variational Methods in Mathematics, Science and Engineering. D. Reidel Publ. Co., Dordrecht, The Netherlands
- [38] Rektorys K (1994) Survey of Applicable Mathematics, Kluwer Academic Publishers.
- [39] Roy K.K (2008), Potential Theory in Applied Geophysics, Springer-Verlag Berlin Heidelberg
- [40] Sansò F, Sideris M (2013) Geoid Determination - Theory and Methods. Lecture Notes in Earth System Sciences, Springer-Verlag, Heidelberg, Germany
- [41] Sansò F and Rummel R (1997) Geodetic boundary value problems in view of the one centimeter geoid. In: Lecture notes in earth sciences, Springer
- [42] Shaofeng B, Dingbo C (1991) The finite element method for the geodetic boundary value problem. Manuscr Geod 16:353359

- [43] Šprlák M, Fašková Z, Mikula K (2011) On the application of the coupled finite-infinite element method to the geodetic boundary value problem, *Studia Geophysica et Geodaetica*, Vol. 55 (2011) pp. 479-487
- [44] Stroustrup B (2013) *The C++ Programming Language (Fourth Edition)*. Addison Wesley. Reading Mass. USA. ISBN 0-321-56384-0. 1360 pages.
- [45] Zeman A (2005) *Fyzikální geodézie. Skriptum*. Vydavatelství ČVUT